NAVAL POSTGRADUATE SCHOOL

MONTEREY, CALIFORNIA

DISSERTATION

IMPROVING WIND-BASED UPWELLING ESTIMATES OFF THE WEST COASTS OF NORTH AND SOUTH AMERICA

by

Mark H. Pickett

December 2003

Dissertation Supervisors: Curtis A. Collins
Franklin B. Schwing

Approved for public release; distribution is unlimited

THIS PAGE INTENTIONALLY LEFT BLANK

REPORT DOCUMENTATION PAGE			Form Approved OMB No. 0704-0188
Public reporting burden for this collection of information is estimated to average 1 hour per response, including the time for reviewing instruction, searching existing data sources, gathering and maintaining the data needed, and completing and reviewing the collection of information. Send comments regarding this burden estimate or any other aspect of this collection of information, including suggestions for reducing this burden, to Washington headquarters Services, Directorate for Information Operations and Reports, 1215 Jefferson Davis Highway, Suite 1204, Arlington, VA 22202-4302, and to the Office of Management and Budget, Paperwork Reduction Project (0704-0188) Washington DC 20503.			
1. AGENCY USE ONLY *(Leave blank)*	**2. REPORT DATE** December 2003	**3. REPORT TYPE AND DATES COVERED** Dissertation	
4. TITLE AND SUBTITLE: Improving Wind-based Upwelling Estimates Off the West Coasts of North and South America			**5. FUNDING NUMBERS**
6. AUTHOR(S) Pickett, Mark H.			
7. PERFORMING ORGANIZATION NAME(S) AND ADDRESS(ES) Naval Postgraduate School Monterey, CA 93943-5000			**8. PERFORMING ORGANIZATION REPORT NUMBER**
9. SPONSORING / MONITORING AGENCY NAME(S) AND ADDRESS(ES) N/A			**10. SPONSORING / MONITORING AGENCY REPORT NUMBER**
11. SUPPLEMENTARY NOTES The views expressed in this thesis are those of the author and do not reflect the official policy or position of the Department of Defense or the U.S. Government.			
12a. DISTRIBUTION / AVAILABILITY STATEMENT Approved for public release; distribution is unlimited.			**12b. DISTRIBUTION CODE**

13. ABSTRACT ***(maximum 200 words)***

Weekly upwelling was estimated at 25 sites off the North and South American west coasts from August 1999 to December 2001 using geostrophically derived winds, model-derived winds from the U.S. Navy's global atmospheric (NOGAPS) model, and QuikSCAT satellite-measured winds. Satellite-measured winds, verified with 15 U.S. west coast buoys, were within 1.3 m s^{-1} and 26° RMS. Upwelling estimates derived from geostrophic winds using the Pacific Fisheries Environmental Laboratory (PFEL) technique were compared to those derived from both satellite-measured winds and model-derived winds. Upwelling estimates from model-derived winds agreed with satellite-based estimates at all 14 North American sites and 9 of 11 South American sites. Estimates from geostrophic winds agreed with satellite-based estimates at 12 of 14 North American sites and 7 of 11 South American sites. These comparisons showed that upwelling estimates based on the Navy's global model winds were accurate in more regions than those based on geostrophic winds. A fine-scale upwelling investigation using the Navy's high-resolution atmospheric model (COAMPS) revealed narrow near-shore bands of strong wind-stress and wind-stress-curl missed in the above upwelling estimates. Improvements in the depiction of coastal upwelling will require wind data and upwelling estimates with at least a 10 km resolution.

14. SUBJECT TERMS Upwelling, California Current, Peru/Chile Current, QuikSCAT, Wind-stress curl, Upwelling Index, Ekman transport, Ekman pumping			**15. NUMBER OF PAGES** 132
			16. PRICE CODE
17. SECURITY CLASSIFICATION OF REPORT Unclassified	**18. SECURITY CLASSIFICATION OF THIS PAGE** Unclassified	**19. SECURITY CLASSIFICATION OF ABSTRACT** Unclassified	**20. LIMITATION OF ABSTRACT** UL

NSN 7540-01-280-5500 Standard Form 298 (Rev. 2-89)
Prescribed by ANSI Std. 239-18

THIS PAGE INTENTIONALLY LEFT BLANK

Approved for public release; distribution is unlimited.

IMPROVING WIND-BASED UPWELLING ESTIMATES OFF THE WEST COASTS OF NORTH AND SOUTH AMERICA

Mark H. Pickett
Lieutenant Commander, National Oceanic and Atmospheric Administration
B.S., West Virginia University, 1983
M.S., University of Miami, 1991

Submitted in partial fulfillment of the
requirements for the degree of

DOCTOR OF PHILOSOPHY IN PHYSICAL OCEANOGRAPHY

from the

NAVAL POSTGRADUATE SCHOOL
December 2003

Author: _____
Mark H. Pickett

Approved by:

_____	_____
Franklin B. Schwing	Curtis A. Collins
NOAA/PFEL	Professor of Oceanography
Dissertation Supervisor	Dissertation Committee Chair
_____	_____
Leslie K. Rosenfeld	Jeffrey D. Paduan
Research Associate Professor	Associate Professor
_____	
Carlyle H. Wash	
Professor of Meteorology	

Approved by: _____
Mary L. Batteen, Chair, Department of Oceanography

Approved by: _____
Julie Filizetti, Associate Provost for Academic Affairs

THIS PAGE INTENTIONALLY LEFT BLANK

ABSTRACT

Weekly upwelling was estimated at 25 sites off the North and South American west coasts from August 1999 to December 2001 using geostrophically derived winds, model-derived winds from the U.S. Navy's global atmospheric (NOGAPS) model, and QuikSCAT satellite-measured winds. Satellite-measured winds, verified with 15 U.S. west coast buoys, were within 1.3 m s^{-1} and 26° RMS. Upwelling estimates derived from geostrophic winds using the Pacific Fisheries Environmental Laboratory (PFEL) technique were compared to those derived from both satellite-measured winds and model-derived winds. Upwelling estimates from model-derived winds agreed with satellite-based estimates at all 14 North American sites and 9 of 11 South American sites. Estimates from geostrophic winds agreed with satellite-based estimates at 12 of 14 North American sites and 7 of 11 South American sites. These comparisons showed that upwelling estimates based on the Navy's global model winds were accurate in more regions than those based on geostrophic winds. A fine-scale upwelling investigation using the Navy's high-resolution atmospheric model (COAMPS) revealed narrow near-shore bands of strong wind-stress and wind-stress-curl missed in the above upwelling estimates. Improvements in the depiction of coastal upwelling will require wind data and upwelling estimates with at least a 10 km resolution.

THIS PAGE INTENTIONALLY LEFT BLANK

TABLE OF CONTENTS

LIST OF FIGURES

LIST OF TABLES

THIS PAGE INTENTIONALLY LEFT BLANK

ACKNOWLEDGMENTS

I would like to thank my advisors, Curt Collins, Frank Schwing, Jeff Paduan, Leslie Rosenfeld, and Chuck Wash for their support and guidance during this study. I also thank the NOAA Corps and the leadership of the NOAA Pacific Fisheries Environmental Laboratory who provided me the opportunity to pursue this goal. I thank my family and friends for their continuous understanding and encouragement when times got tough. I could not, nor would I have tried to, take on this work in addition to an already demanding sea-going career without the help and support of my loving wife Karen. She has paid dearly with missed time together and I promise to make that up to her during the remaining years of our lives. Lastly, I want to thank my father Robert Pickett. Ever since I was a young boy I wanted to grow up to be as intelligent, generous, gracious, and understanding as he is. During this study, he spent nearly as much time editing my papers and checking my work as I did. I could not have done it without him. He taught me much more than he could ever know. I hope that someday I can be just like him.

THIS PAGE INTENTIONALLY LEFT BLANK

EXECUTIVE SUMMARY

The National Oceanic and Atmospheric Administration's Pacific Fisheries Environmental Laboratory (PFEL) provides monthly upwelling estimates at specific sites off the west coasts of North America and South America. The purpose of these estimates, called upwelling indices, is to highlight regions of high biological productivity in eastern boundary currents. The North American sites range from 21°N (off Cabo San Lucas in Baja, California) to 60°N (off the Kenai Peninsula, Alaska), and span the entire California Current system. The South American sites are between 15°S (near Lima, Peru) and 45°S (off southern Chile), and are within the Peru-Chile Current system. The North American upwelling estimates have been published continuously since 1946 (monthly since 1946, daily since 1967), and the South American estimates since 1981.

The coastal regions covered by these upwelling estimates produce 20% of the world's total marine fish catch (Food and Agriculture Organization of the United Nations, 1995). From 1994 to 1998 the average annual catch in these regions was 8 million metric tons of anchovy (*Engraulis mordax, E. ringens*), 2 million metric tons of mackerel (*Scomber japonicus*), and 1 million metric tons of sardine (*Sardinops sagax*). In addition, these smaller species attract commercially important predators such as tuna (*Thunnus spp., Euthynnus pelamis*), swordfish (*Xiphias gladius*), and salmon (*Oncorhynchus spp*.). These predators also provide significant local economic impact due to sport fishing.

Since these areas are so productive, there has long been a demand for information on the locations and times of strong upwelling events. To satisfy this demand, PFEL began producing monthly estimates using the Bakun (1973) method. First, a monthly mean surface pressure field was calculated by averaging available surface pressure analyses. Next, a monthly mean geostrophic wind vector was estimated at each site using this pressure field. This wind vector was then used in a simple bulk stress formula, with a constant drag coefficient, to estimate wind stress at each specific site. Finally, the shore-parallel component of this wind stress was used to estimate offshore Ekman transport. This offshore transport was used as the upwelling estimate and published as the PFEL index for that particular site.

Although the above calculations involved a host of assumptions and approximations, the results turned out to be valuable. First, they are the only routinely produced upwelling estimates for these areas. Second, they have been published using the same methods and data sources for nearly 60 years for North America and over 20 years for South America. As a result, they provide long-term data to relate upwelling to catch variability in various fish species. The usefulness of these estimates is evident in that they have been referenced in over 400 fisheries and oceanographic publications. Since these upwelling estimates are so heavily used, an obvious question is: How accurate are the present upwelling indices, and can their accuracy be improved using better wind data than geostrophic estimates?

To provide a reference data set for these upwelling comparisons, QuikSCAT satellite-measured winds were used. QuikSCAT is in a polar orbit 500 miles above the earth, and uses a rotating, dual-beam, microwave radar for estimating ocean surface wind speed and direction. Wind measurements were available every 12 hours at each upwelling site.

In the first phase of this three-part study, satellite-measured winds were verified by comparing them to coastal buoy wind observations. The results of this work, discussed in Section II, showed that the QuikSCAT satellite provides accurate coastal wind measurements. Once the satellite wind measurements were validated, they were then used to generate a reference set of upwelling estimates. Although this satellite was ideal for this application, long-term applications are uncertain because QuikSCAT is well past its design lifetime. A more permanent source of wind data will be required for similar upwelling tests in the future.

In the second phase of this study, model-derived winds were substituted for the geostrophic-derived winds presently used in the PFEL upwelling method to see if they offered advantages. The model chosen was the U.S. Navy's global atmospheric model which has been used to produce six-hourly wind data since 1988. Weekly averaged upwelling estimates for both model-derived and geostrophic-derived winds were compared by matching them both to the reference set based on satellite-measured winds. Comparisons were run from August 1999 through December 2001 at 14 sites off the

North American west coast and 11 sites off the South American west coast. The results, outlined in Section III, showed that when model-based winds were used in PFEL upwelling estimates, higher predictive skill scores were achieved at more sites than with estimates based on geostrophic winds.

Even though winds from the Navy global model improved PFEL upwelling estimates, its 100-km horizontal resolution missed major coastal wind features. The importance of these missed features was revealed in the third phase of this study which employed the Navy's high-resolution research model. This model, first verified with satellite and buoy data, was run from May 1999 to September 2000 to provide a 9-km grid of wind data off the North American west coast. Results, detailed in Section IV, indicated that upwelling effects of strong, small-scale wind stress and wind-stress curl are either missed or aliased in both the global wind model and in the PFEL upwelling indices.

THIS PAGE INTENTIONALLY LEFT BLANK

I. INTRODUCTION

A. THE PROBLEM

Coastal upwelling estimates are important to the U.S. Navy and to the National Oceanic and Atmospheric Administration (NOAA) as well as many foreign agencies. The Navy is interested because upwelling radically alters the thermal, optical, and acoustic properties of coastal waters, and contributes to fog formation. These upwelling-induced conditions impact Naval coastal operations which in recent years have become increasingly important in regional conflicts. Hence a better method for estimating upwelling would be of direct benefit to fleet operations.

NOAA is likewise interested in coastal upwelling estimates. These estimates not only support their general mission to understand near-shore processes, but also support their specific mission to manage marine fisheries. Fisheries in eastern boundary currents are heavily dependent on upwelling events which bring nutrient rich waters to the surface. Biological productivity soars during these events which, in turn, support large fish populations. Because of such upwelling events, the coastal zones off the west coasts of North and South America alone provide 20% of the world's total marine fish catch (Food and Agriculture Organization of the United Nations, 1995).

Near-shore, wind-driven upwelling is typically produced in one of two ways. The most common way requires an alongshore wind that, in conjunction with the earth's rotation, moves surface waters offshore. This process, called Ekman transport, can force surface coastal water downward, or bring nutrient-rich deeper water upward. The second process, called Ekman pumping, occurs as wind-stress curl generates ocean-surface divergence, or convergence, which forces water upward or downward. Although the effects of both of these upwelling processes have been well observed, direct measurements are very difficult. Vertical velocities are typically only a few meters per day, and hence beyond the capabilities of most current meters.

Since there was a strong interest in the times and locations of coastal upwelling events, the NOAA Pacific Fisheries Environmental Laboratory (PFEL) developed a method for estimating these events (Bakun, 1973). Routine surface wind data were

unavailable when the estimates were started, so PFEL resorted to indirect estimates deduced from large-scale geostrophic calculations. These indirect wind estimates were then used in a simple transport equation (Ekman, 1905) to estimate upwelling. Based on this approach, PFEL started routinely calculating and distributing coastal upwelling estimates. Their estimates, which they call upwelling indices, are the only regularly produced upwelling data for the North and South American west coasts. Even though their technique relies on large-scale geostrophic wind estimates and ignores smaller-scale effects, PFEL upwelling indices have proved useful. They have been referenced in over 400 fisheries and oceanographic publications.

In recent years, however, there have been major improvements in coastal wind data. Satellites can now measure surface winds over all ocean areas. Also, global atmospheric models have made great strides in accuracy as more observations have been assimilated, and computer capabilities have allowed better resolutions. In light of these advances, this study was designed to examine historical upwelling estimates and to investigate the effect of better wind data on these estimates. The selected test regions were the coastal zones off the west coasts of North and South America.

B. COASTAL UPWELLING

Historical upwelling estimates have been based on the simple Ekman transport equation:

$$M_n = \tau_p / f$$

where M_n is the Ekman transport normal to the coast, τ_p the wind stress parallel to the coast and f the Coriolis parameter. Mass transport derived from this equation is per unit width of coastline and is directed perpendicular to the wind's direction (to the right in the northern hemisphere, left in the southern). There are many assumptions involved in deriving this equation. For example, it is assumed that the ocean is homogeneous, boundless, infinitely deep, and exposed to a steady, uniform wind. It is also assumed that the internal friction, or eddy viscosity, is constant with depth and the ocean is in a steady state. Although the above assumptions are often violated, numerous observational studies

have shown that transport calculated from this simple equation agrees well with measured cross-shelf transport over timescales greater than a day (Smith, 1981; Lentz, 1992; Chereskin, 1995).

Wooster and Reid (1963) did an investigation of coastal upwelling in the five major eastern boundary currents (California, Peru, Benguela, Canary, and West Australia currents). By using five-degree wind stress fields and the Ekman transport equation, they calculated seasonal and geographical estimates of coastal upwelling. A mean alongshore wind component was calculated over each five degree segment of coastline, and offshore transport was calculated over each season. In their survey, Wooster and Reid noted that mean wind stress over a five-degree area was probably a poor approximation of actual stress, but they nevertheless concluded that these offshore transports seemed to provide reasonable estimates of upwelling in the five eastern boundary currents.

Smith (1968) reviewed upwelling dynamics for both steady and transient state conditions. He concluded that offshore Ekman transport was closely related to vertical velocity at the bottom of the surface layer. He also noted, however, that this transport never occurred in isolation since other coastal currents were always interacting, especially at time scales of a day or shorter. Moreover, offshore transport itself invokes other currents by redistributing water masses. As water is pushed offshore, a pressure gradient develops that generates a coastal geostrophic current. In spite of these confounding factors, however, Smith concluded that the width of offshore Ekman transport depends on vertical stratification and on latitude, and that this transport can provide a reasonable estimate of mean vertical-velocity within the surface layer, even in early stages of upwelling.

Lentz (1992) used data from several wide-ranging observational studies of coastal upwelling (off Oregon, northwest Africa, Peru, and northern California) to study wind stress and surface boundary layer currents. Based on wind, current, and temperature measurements from surface buoys, moored instruments, and conductivity-temperature-depth sensors, he found that during the upwelling season all four regions had mixed layers less than 20 m deep. He also pointed out that layer depth fluctuated primarily at the diurnal period and at periods greater than 36 hours. In the case of the longer periods,

mixed layer depth varied with mean surface wind stress, and was not strongly dependent on either surface heat flux or advection. He also used current data from each region to measure cross shelf transport at periods greater than 36 hours. He then showed that such measurements agreed well with Ekman transport derived from surface wind measurements and the variable drag coefficient of Large and Pond (1981).

Although Lentz's results provided strong support for using offshore Ekman transport as an index of coastal upwelling, there are some locations where it does poorly. One is off the western Australian coast where there is little indication of upwelling in spite of strong, persistent, alongshore winds. In this particular case, an unrelated geostrophic flow overwhelms the wind-induced offshore flow that normally generates upwelling (Smith et al. 1991). Another example is off the Peruvian coast during the 1982 and 1983 El Niño event. Even though there were persistent alongshore winds, there were no surface manifestations of upwelling. Surface waters were warm and nutrient poor. In that case, a very deep thermocline blocked the normal surface occurrence of cool, nutrient rich water (Huyer et al., 1987). These two examples show that although Ekman transport may be a good indicator of vertical velocity, it is not necessarily a good indicator of surface water enrichment.

Despite these exceptions, if one can accurately observe or predict mean coastal wind fields on the time scale of several days, then offshore Ekman transport calculations provide an effective method for estimating coastal upwelling.

C. PFEL UPWELLING ESTIMATES

1. Original Method

In 1973, PFEL began routinely publishing monthly upwelling indices at North American coastal sites (between 21°N and 60°N, Figure 1). They also provided upwelling hind-casts at these sites all the way back to 1946. South American sites (between 15°S and 45°S, Figure 2) were added in 2001, with hind-casts back to 1981. All of these estimates are still being published at the same sites, and PFEL has remained with basically the same upwelling computational method.

The method was developed by Bakun (1973) and is based on the work of Fofonoff (1962). Fofonoff originally developed Ekman transport estimates for the North

Pacific using mean sea-level pressure fields obtained from the United States Weather Bureau. Although Fofonoff used these estimates to study ocean circulation, Wickett (1967) found they could be used to study zooplankton concentrations off California and in the western Bering Sea. He found that there was a relationship between zooplankton concentrations and the north-south component of Ekman transport in the Gulf of Alaska. Bakun was working on coastal upwelling at the time and, based on Wickett's results, decided to compute the offshore component of Ekman transport for specific sites off the North American west coast. Bakun referred to this offshore component as a coastal upwelling index. His method has proved to be easy to use, and has provided valuable data that are still widely used and referenced today.

The first step in Bakun's method, adopted by PFEL, was to obtain a surface pressure field. Pressure fields were used because they were the only consistently available surface data when the index was developed. From 1946 to 1962 PFEL acquired hand or machine analyzed monthly pressure fields from either the National Climate Center or the National Center for Atmospheric Research. Since 1962 pressure fields have been acquired exclusively from the U.S. Navy's Fleet Numerical Meteorology and Oceanography Center (FNMOC). Data were originally provided on a polar-stereographic projection that had to be extrapolated to a three-degree grid in a spherical coordinate system to standardize the grid interval. In the early 1970's FNMOC began using atmospheric models with standardized grids to produce the surface pressure fields used in the upwelling index. In the late 1980's FNMOC made significant enhancements to their atmospheric model and began to produce operational surface wind fields. However, these early surface wind fields were not as reliable as the well established surface pressure fields. Therefore, PFEL decided to maintain continuity in the upwelling index by continuing to use surface pressure fields to calculate the upwelling index.

Once these pressure fields were obtained, surface pressure gradients were calculated by dividing pressure differences by the distance between grid points. These pressure gradients were then used in geostrophic calculations to estimate a monthly mean surface wind vector. To allow for friction, this vector was rotated 15° to the left (to the

right in the southern hemisphere) and reduced in magnitude by 30%. This process was repeated at each upwelling index site.

The friction-modified geostrophic winds at each site, as estimated above, were then converted to wind stress using a simple bulk stress formula:

$$\vec{\tau} = \rho_a C_d |\vec{v}| \vec{v}$$

where $\vec{\tau}$ is the wind stress vector, ρ_a the air density, C_d an empirical drag coefficient, and $\vec{v}$ the estimated wind vector near the sea surface with magnitude $|\vec{v}|$. A value of 0.0026 was used for the drag coefficient to calculate the wind stress from the monthly mean fields. Nelson (1977) and Davidson (1974) point out that such a large C_d is necessary because monthly averaging smoothes all synoptic-scale variability.

The surface wind stress values were next used to calculate Ekman transport at each site. Finally, the offshore component of this transport was determined by calculating the dot product of the transport vector with an orthogonal drawn to a three-degree (of latitude) segment of the local coastline. This offshore component of the transport vector was used as the monthly mean upwelling index for each of the sites. The purpose of this index was to estimate mean vertical velocity at the base of the Ekman layer. Thus a positive value of the index implied offshore transport (upwelling), and a negative value implied onshore transport (downwelling). The index is in units of cubic meters per second per 100 meters of coastline (equivalent to metric tons/sec/100m of coastline) and is intended to represent monthly mean upwelling along the adjacent 300 km section of coastline. Also, any index value can be converted to vertical velocity simply by dividing by the Rossby radius, which is the approximate offshore scale of the transport (Allen, 1973). Details of the method, assumptions, and calculations are in Bakun (1973), Schwing et al. (1996), and Norton et al. (2001).

2. Recent Updates

To include contributions at smaller time and space scales, PFEL began using six-hourly surface pressure fields in 1967, and one-degree surface pressure grids in 1994. Upwelling, calculated on these finer scales, was then averaged and published as daily, weekly, and monthly indices. These improvements were possible because of the

increased resolution of the Navy's atmospheric model. Also, after switching to six-hourly pressure fields the drag coefficient was reduced to the more commonly accepted value of 0.0013.

In January 2001, PFEL added a web site (http://las.pfeg.noaa.gov/las/main.pl) that allowed users to estimate upwelling at any location in the world. The same technique was used, but the drag coefficient was updated to a non-linear form based on Large and Pond (1981) with a modification for low wind speeds by Trenberth et al. (1990). The effect of all the above updates depends heavily upon the location, pressure gradient, wind speed, grid size, and coastal proximity of any particular site.

3. Limitations

The Bakun method described above requires a number of assumptions and approximations. For example, there are assumptions inherent in estimating surface wind via geostrophy. Geostrophic calculations require a frictionless, homogeneous atmosphere with steady state, straight-line flow. These assumptions may be reasonable in the open ocean, but near-shore winds are known to steer dramatically around coastal mountains (Dorman et al., 2000). Also, after a geostrophic wind is calculated, the constant friction applied to estimate surface wind (15 degree rotation, 30% speed reduction) neglects modifications caused by air-sea temperature difference and surface roughness. Halliwell and Allen (1987), for example, compared geostrophic-derived surface wind directions to those measured by buoys and found that differences ranged from 5° to 50° off the North American west coast.

Wind stress based on monthly mean pressure fields presented another error. The stress is underestimated by an amount proportional to the variability of the pressure field according to Nelson (1977). He showed that off California, stress derived from a monthly mean pressure field underestimated the mean stress based on 6-hourly pressure fields by more than 50%. This problem was rectified in 1967 when the index was derived using 6-hourly surface pressure analyses, and then averaged over daily, weekly, or monthly intervals.

Another problem stemmed from the original use of 3-degree surface pressure grids. The north-south component of geostrophic wind near the coast often had to be computed with one grid point over land. This caused a pressure gradient discontinuity

due to the coastal mountains and resulted in overestimates of alongshore wind (Bakun, 1973). The problem was reduced in 1994 when the wind was extracted from a one-degree surface pressure grid.

Another possible source of error in the Bakun method was the constant drag coefficient used to convert surface wind to wind stress. Many studies (e.g., Large and Pond, 1981; Smith, 1988) have shown that drag coefficients vary with both wind speed and air-sea temperature difference. As mentioned above, an attempt to minimize this possible error is being tested presently on the PFEL web site by applying a more realistic wind-speed-dependent drag coefficient.

And finally, there are problems with the method near the equator. Within roughly 10-degrees of the equator the Coriolis force becomes so small that the geostrophic assumption is no longer valid and transport calculations must include friction (Ward and Hoskins, 1996; Xie and Hsieh, 1995).

D. OTHER UPWELLING ESTIMATES

Although the technique for estimating upwelling developed by Bakun and used by PFEL is the best known, other methods are available. Some are extensions or modifications of the Bakun technique, and others are based on different data inputs. For example, Hsieh et al. (1995) extended the upwelling technique back to 1899 with historical monthly pressure data from the National Center for Atmospheric Research. They then demonstrated the value of these estimates by correlated them with records of the percentage of body fat of sardines and with the weight of herring caught off British Columbia, Canada.

Thomson and Ware (1996) used current meters at several depths to develop an upwelling index based on alongshore current that they called a velocity index. Since alongshore current is related to the cross-shore density field, they suggested their index could be used as a gage of upwelling intensity. They found that their velocity index had less variability than the PFEL index, and suggested that the Bakun method was too sensitive to wind variations with periods less than a few days. They concluded that their index was a more accurate gage of coastal upwelling.

Kuo et al. (2000) based their upwelling index on surface temperature differences. Sea surface temperature and wind stress were extracted from satellite radiometer and scatterometer data. Temperature differences from the radiometer were used to outline the upwelling areas, and wind stress from the scatterometer was used as an indicator of upwelling depth. They also estimated differential heat loss between the cooler upwelling water and the surrounding water. This method has obvious appeal because all data were obtained from satellites with their global coverage.

Although some of the above upwelling estimates may offer potential advantages over the PFEL technique, they all require both elaborate and expensive instrumentation or data sources that are not continuously available. A major advantage of the PFEL index is that the only data required, atmospheric surface pressure, is routinely available from many sources worldwide.

E. FISHERIES APPLICATIONS

As mentioned earlier, upwelling ecosystems off the west coasts of North and South America are very productive. The dominant commercial species include anchovy, jack mackerel, chub mackerel, and sardine. From 1994 to 1998 the average annual catch in these regions was eight million metric-tons of anchovy, four million metric-tons of jack mackerel, two million metric-tons of chub mackerel, and one million metric-tons of sardine. In addition, the prevalence of these smaller species attracts commercially important predators such as tuna, swordfish, and salmon. These larger fish also attract sport fishing which provides significant local economic impact. These catches are sustained by the continuous supply of nutrients that are carried to the surface by coastal upwelling. Obviously, accurate prediction of the upwelling that carries these nutrients would help fisheries managers monitor these economically important fish stocks.

To be valuable to fisheries management, upwelling indices must not only depict vertical nutrient flux, but they should also have a well-documented relationship with fisheries production. Studies described earlier have shown that offshore Ekman transport, the basis of the PFEL index, is related to vertical velocity at the bottom of the surface layer. In addition, over 400 published studies have used the index as an indicator of Ekman transport, nutrient fluxes, or fisheries production.

Nutrient flux studies by Bakun and Parrish (1982) off both North and South American west coasts found that upwelling variations within each year control the concentration of food organisms as well as the location and time of spawning. They also found that too much offshore transport carries nutrients and larvae away from near-shore nursery areas. As evidence, they noted that spawning areas in both the California and Peru Current systems are located downstream from maximum upwelling regions rather than within them. Brodeur and Ware (1992), in another nutrient study, found significant correlations between long-term records of the PFEL index and zooplankton concentration in the northern Gulf of Alaska.

Parrish and Mallicoate (1995) correlated the PFEL index to relative fish weight (weight divided by average weight of fish of the same length) using catch data from the Southern California Bight. They found that the relative weight of both mackerel and jack mackerel correlated with the upwelling index off central Baja California, a region know to transport nutrients to the Bight by near-shore surface currents (Casey et al., 1986). More recently, Koslow et al. (2002) used adult Coho salmon returns in the California, Oregon, and Washington rivers to calculate a significant correlation between adult coho salmon survival and the PFEL index. From this correlation they concluded that upwelling is one of the most important factors in the marine survival of young coho salmon.

Although the above studies have had success in correlating the PFEL index with nutrient supply and fisheries productivity, other studies (Gargett, 1997; Ryding and Skalski, 1999; Botsford et al., 2003; Stenevik, et al., 2003) have suggested that such correlations are not strong because the relationship is nonlinear. Cury and Roy (1989), for example, showed that maximum reproductive success of several species occurred only in moderate wind speeds. They found a dome-shaped relationship between the upwelling index and recruitment of both Peruvian anchovies and Pacific sardines.

The above studies have confirmed that nutrient supply and fisheries productivity are correlated with the PFEL upwelling index. Regardless of whether the underlying relationships are linear or nonlinear, the studies demonstrate that the PFEL index is a widely accepted and useful tool in fisheries management.

F. STUDY OBJECTIVES

Since the PFEL upwelling indices are so well known and accepted, this study was designed to test and hopefully improve their accuracy. The PFEL technique relies on surface winds to calculate the offshore component of Ekman transport used in the index. Any attempt to improve the technique, therefore, requires an increase in the accuracy of surface wind data. Wind is the only variable used in the calculation, and it is squared. Hence small errors in the wind can translate into large errors in the upwelling index. Geostrophic-derived winds, presently used in the estimates, are susceptible to errors since they involve assumptions and approximations that are rarely satisfied near-shore.

Any new source of wind data needs to be first verified with an accurate coastal wind sensor. For this study that sensor was the QuikSCAT satellite launched in 1999 by the National Aeronautics and Space Administration (NASA). This satellite provides global wind measurements averaged over each 25 km area of ocean. It is in polar orbit 500 miles above the earth, and measures wind speed and direction with a rotating, dual-beam, microwave radar. Wind measurements are available at any location approximately once every 12 hours. Tests have shown the satellite's wind data to be within 1.0 m/s and 20° RMS in offshore regions (Ebuchi et al., 2002). Near-shore accuracy, where coastal interference limits the view, was unknown.

For the first phase of this study, therefore, the near-shore accuracy of satellite-measured winds had to be established by comparing them to buoy measurements of known accuracy. The results, discussed in Section II, showed that the satellite can provide near-shore wind measurements within 1.3 m/s and 26° RMS. Even though this satellite is now well past its design life, it performed flawlessly during the entire year and a half test period.

After the satellite-measured winds were verified, the second phase of the study was to find and test a consistent source of coastal wind data for comparison with the presently used geostrophic-derived data. This alternate source was provided by the U.S. Navy global atmospheric model (NOGAPS). The model had several apparent advantages over geostrophic-derived winds: it used full-scale dynamics, winds were available all the way to the equator, and more realistic variable friction was used.

This particular Navy model has been used to produce 12-hourly wind analysis and 6-hourly forecasts since 1988, but has undergone major advances since then. In 1994 the Navy increased the horizontal resolution from 300 to 100 km, and data assimilation was improved by adding more complex quality control.

Before using the above model, the surface wind data was first verified with measurements. Buoy wind observations could not be used, as they were for the satellite, because they were already assimilated into the model. Instead, the model was verified using satellite wind observations off the North and South American west coasts. The results showed that weekly averaged model wind data matched satellite wind data within 1.7 m/s and 31° RMS based on two and a half years of observations at 25 separate sites.

After the model-derived winds were tested, upwelling calculations using the PFEL technique were done with all three sets of wind data: satellite-measured, model-derived and geostrophic-derived. Weekly averaged upwelling estimates from the three wind data sets were compared from August 1999 through December 2001 at 14 sites off the North American west coast and 11 sites off the South American west coast. The results, outlined in Section III, showed that model-derived winds resulted in improved upwelling estimates when compared to those based on geostrophic-derived winds.

The last phase of this study was to investigate the role of mesoscale wind-stress curl on upwelling in the coastal region. For this part of the study, the Navy's mesoscale meteorological model (COAMPS) was run for the U.S. west coast using a 9-km grid. This model was implemented in 1999, and Dorman et al. (2000) showed that it accurately reproduced wind-fields disturbed by coastal promontories off the west coast of North America. Before the model was used for this study, however, it was first verified with satellite and buoy data. After verification it was run from May 1999 to September 2000.

Next, the model's high-resolution wind data were used to calculate offshore transport and vertical velocity at each 9-km grid point in the California Current system. The results, detailed in Section IV, showed that at such a fine scale an entirely different picture of coastal upwelling emerges. Features of wind and upwelling were delineated that would be missed or aliased by estimates based on coarser resolution wind data. Among these features were areas of strong, small-scale wind-stress curl around coastal

promontories. These wind-stress curl areas would generate another upwelling process, called Ekman pumping, which turned out to be comparable in magnitude to offshore Ekman transport. Overall, the pattern of upwelling, offshore transport, and vertical velocity that emerged from high resolution model winds was entirely different from that deduced for the same area and time using winds from the 100-km grid model.

In summary, the objective of the three phases of this research was to provide a better understanding of coastal upwelling and to suggest an improved technique for estimating that upwelling in any of the world's coastal zones. Although upwelling indices based on geostrophic-derived winds are reliable in many locations, by using model-derived wind data more accurate estimates can be obtained with the present PFEL method. To produce a more realistic and detailed picture of coastal upwelling, however, wind data with at least a 10 km resolution are necessary so that all scales of upwelling features and processes can be evaluated.

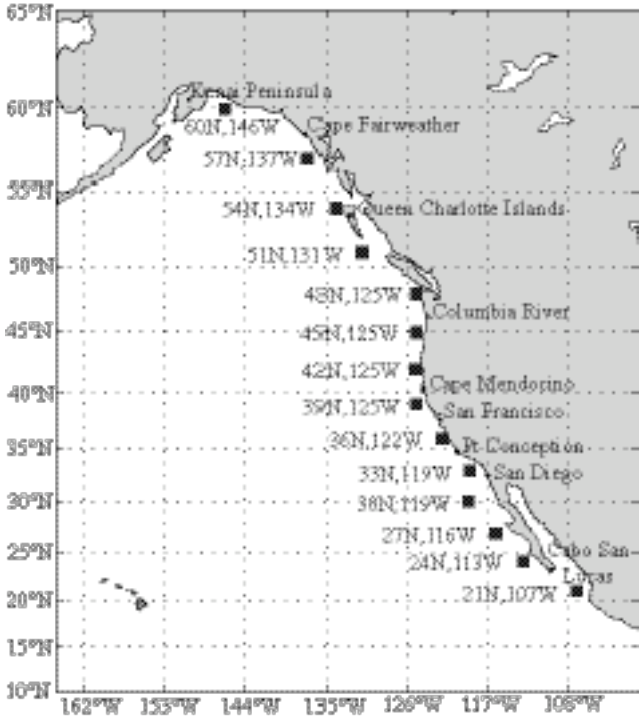

Figure 1. Locations of the 14 North American upwelling sites used in this study. The sites range from 21°N to 60°N and from 25 km to 275 km from shore.

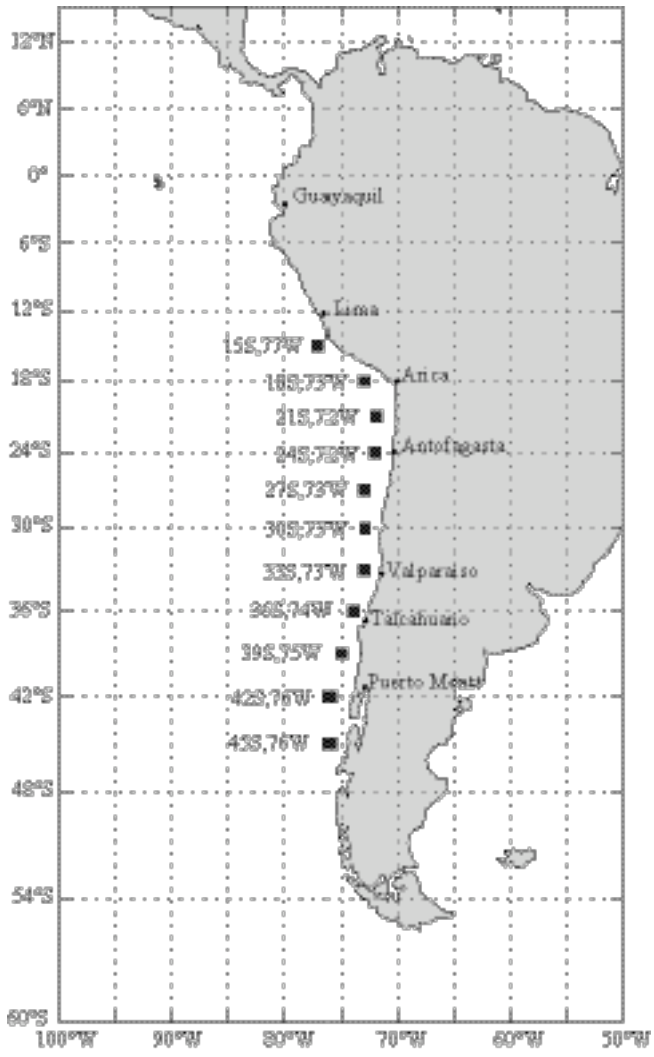

Figure 2. Locations of the 11 South American upwelling sites used in this study. The sites range from 15°S to 45°S and from 110 km to 190 km from shore.

THIS PAGE INTENTIONALLY LEFT BLANK

II. QUIKSCAT SATELLITE COMPARISONS WITH NEAR-SHORE BUOY WIND DATA OFF THE US WEST COAST[1]

A. BACKGROUND

During the past 20 years numerous studies have demonstrated the ability of satellite-borne radar to measure ocean winds. This type of instrument was used on the Seasat Scatterometer System (SASS), the National Aeronautics and Space Administration (NASA) Scatterometer (NSCAT), and the European Remote Sensing satellites (ERS-1 and 2). Freilich and Dunbar (1999) assessed NSCAT's wind accuracy by comparing satellite-derived swath data to 43 buoys located off the US east and west coasts. They excluded the near-shore west coast buoys because of low correlations, but found root-mean-square (rms) wind differences offshore of 1.3 m s^{-1} and 17 degrees.

The latest of the wind-measuring satellites, NASA's QuikSCAT, was launched into orbit on 19 June 1999 after an unexpected early termination of NSCAT. QuikSCAT is in polar orbit approximately 500 miles above the earth's surface. The satellite completes its orbit in 101 minutes, and as this orbit migrates around the earth each ocean region is over flown once every 12 hours. For the US west coast, daily over-flights are within 90 minutes of 0200 and 1400 UTC (universal time, coordinated). However, because of the satellite's limited viewing area and the earth's rotation, various sections of the coastal zone are only observed every few days. A rotating, dual-beam, microwave (13.4 gigahertz) radar aboard the satellite measures ocean backscatter. The backscatter is then sent to ground processing stations, where a series of algorithms are used to estimate wind speed and direction at 10 m above the ocean surface under neutrally stable conditions (Liu and Tang 1996). The mission requirement was to provide winds with an rms error of 2 m s^{-1} and 20 degrees.

The raw data from QuikSCAT are collected and managed by NASA's Jet Propulsion Laboratory (JPL). Winds from these data are provided by a number of agencies in several formats. The most commonly used data sets are: near-real-time (NRT) swath data distributed by the National Oceanic and Atmospheric Administration

[1] Published in the Journal of Atmospheric and Oceanic Technology, Vol. 20, No. 12, pp. 1869-1879, 2003.

(NOAA), scientifically processed (Level 2B) swath data administered by NASA's Physical Oceanography Archive Center, and the gridded near-real-time and gridded science data sets produced at the JPL. These JPL gridded data sets, as well as a few other gridded products, for example those produced by the Center for Ocean-Atmospheric Prediction Studies at Florida State University, and the Remote Sensing Systems in Santa Rosa, California are based solely on satellite data, whereas some gridded data sets use QuikSCAT data blended with other sources.

The QuikSCAT satellite is expected to remain operational and provide wind data until the summer of 2004. More information on the satellite, sensor, and data processing is in the QuikSCAT Science Data Product User's Manual (JPL 2001), on the NOAA web site (http://manati.wwb.noaa.gov/quikscat), and on the NASA web site (http://podaac.jpl.nasa.gov/quikscat).

Ebuchi et al. (2002) did an initial evaluation of the QuikSCAT swath data. They compared winds from the scientifically processed swath data to those from offshore buoys using the satellite's first year and a half of wind data. They found that by removing observations both in rain and when buoy winds were less than 5 m s^{-1}, swath data were accurate enough to meet mission requirements. After their editing, they obtained rms differences of 1.0 m s^{-1} and 20 degrees.

Liu et al. (2000) and Xie et al. (2001) demonstrated the value of the JPL's gridded data set. Liu showed that this data set was capable of depicting tropical instabilities near the equator, and Xie used the data set to observe a wind-wake trailing westward behind the Hawaiian Islands.

Since these initial studies demonstrated the satellite's value as a global oceanic wind sensor, a similar instrument was launched in December 2002 on the Japanese Advanced Earth Observation Satellite (ADEOS-II). Before its launch, several studies focused on improving the data processing. Spencer et al. (2000) proposed a signal-processing technique that relied on frequency sweeping or chirping of the scatterometer to increase spatial resolution. This technique, called range slicing, can more finely segment the antenna footprint for better resolution. Portabella and Stoffelen (2001) showed that rain artificially increased satellite wind speed data, and that for rain over 6

mm/hr QuikSCAT data are unusable. Based on these findings, they proposed that a quality index be included with rain-contaminated data sets. Patoux and Brown (2001) suggested an indirect method for analyzing satellite-derived winds by first using the satellite's output to estimate the pressure field. This indirect method allowed them to correct for direction ambiguities, as well as rain and missing data.

Up until now, investigators have focused on QuikSCAT wind data over open-ocean regions where they are valuable for improving operational weather forecasting and monitoring tropical cyclones. Our interest, in contrast, is in wind data within 100 km of the coast. QuikSCAT offers great potential here since it samples all the world's coastal zones twice a day. Hence, we decided to investigate the accuracy of QuikSCAT's near-shore wind data.

Providing accurate wind data near-shore from satellites is challenging. First, data are unavailable very close to shore because any land within the satellite's viewing area contaminates the return signal. Second, land-sea breezes and shore topography produce small space and time scale wind variations that can be smoothed by the satellite's space-averaging, and aliased by the satellite's twice a day sampling. Halliwell and Allen (1987) and Dorman and Winant (1995), for example, recorded just such wind variations using buoy data off the US west coast. Although their data showed the usual large-scale synoptic atmospheric systems, they also found near-shore wind fluctuations with spatial scales of 1 to 10 kilometers and time scales around one day. Dorman and Winant confirmed the variability of these near-shore winds by showing spectral peaks at the diurnal and semi-diurnal frequencies.

The complexity of near-shore winds is one of the prime reasons why the regions are so important. For example, over one-third of the total marine fish catch occurs within this near-shore zone (FAO 1995). Strong alongshore winds drive episodes of upwelling, which in turn lead to intense biological productivity. If the QuikSCAT satellite were able to accurately measure these near-shore winds, then its data would be useful in estimating coastal upwelling. We felt that we could make reasonable estimates of upwelling with the ability to measure coastal winds greater than 4 m s^{-1} to within 1 to 2 m s^{-1} and 30 degrees. Thus, in spite of the challenge of using near-shore satellite wind data, the global coverage

and the potential for estimating upwelling prompted our evaluation. We selected the US west coast for our test site because it is an active upwelling area with a large number of coastal buoys. Our intent was to answer three questions:

1) How large are the near-shore errors in three of the commonly used QuikSCAT wind data sets?

2) Can post-processing reduce these errors?

3) Are any of these data sets accurate enough for coastal upwelling studies?

In an attempt to answer the above questions, wind data from three satellite data sets were compared to data from 12 coastal and 3 offshore buoys from August 1999 to December 2000. The locations of the buoys are shown in Figure 3, and their properties given in Table 1. The three satellite data sets tested were: NASA's scientifically processed swath data, JPL's gridded near-real-time data, and JPL's gridded science data.

B. DATA

1. Satellite

The satellite's dual-beam radar irradiates an elliptical area (25 km across the satellite's path, 37 km along the path) called the instantaneous field of view (IFOV). The rotating antenna and satellite's orbit combine to move this field of view in a cycloid that extends 900 km on each side of the satellite's path. As a result of this dual-beam sweeping action, QuikSCAT provides wind data over approximately 90% of the world's oceans every day. This coverage is a significant improvement over previous satellites (41% coverage for ERS, 77% coverage for NSCAT), but like all polar-orbiting satellites, observations are unevenly distributed in both time and space.

Backscatter from each instantaneous field of view is subdivided into ten slices. Slices from overlapping current and previous across-track sweeps of the radar beam are then combined and averaged to provide 25 km by 25 km wind vector cells (Figure 4). Output is not used if any slice is contaminated by land, so QuikSCAT wind data are masked, and therefore not available, within 30 km of the coast.

The swath data set used in this study is referred to by NASA as QuikSCAT Level 2B. It is provided as 72 wind vector cells (WVC) across the satellite's path, and 1,624 wind vector cells along its path. Each wind vector cell contains up to four possible wind vector solutions. These solutions are ranked according to a maximum-likelihood

estimator based on the backscatter measurements (Long and Mendel 1991). From this ranking, a single wind vector is then selected using an ambiguity removal algorithm. This algorithm employs a modified median filter technique (Shaffer et al. 1991) that makes a selection based on three factors: ranking from the maximum likelihood estimator, consistency with a National Centers for Environmental Prediction (NCEP) numerical weather product, and agreement with the surrounding (7 x 7) wind vector cells. Near shore the relatively low resolution (one-degree) of the numerical weather product and the lack of surrounding cells on the shore side of the wind vector cell may reduce the effectiveness of the modified median filter.

Each swath wind vector cell also has an attached rain flag. Several different techniques are available to produce these rain flags (e.g., Mears et al., 2000; Huddleston and Stiles, 2000). For this study, we used the default thresholds on the standard multidimensional histogram (MUDH) rain flag described in QuikSCAT Users Manual (JPL, 2001). This rain flag works by evaluating specific rain-sensitive backscatter parameters to estimate rain probability in each wind vector cell. High rain probability cells are then compared with the surrounding (5 x 5) wind vector cells. This is done to determine if there are a sufficient number of high probabilities among neighboring cells to warrant the rain flag.

In contrast to the unevenly distributed swath data, gridded data sets are intended to provide winds for large-scale, quasi-synoptic analysis. Various techniques (Cressman 1959; Koch et al. 1983; Tang and Liu 1996; Liu et al. 1998) are employed to overcome the irregular time and space sampling of satellite wind data. These techniques are best suited for large time and space scales. The inherent time and space aliasing is usually dealt with by averaging. For example, Schlax et al. (2001) demonstrated that sampling errors on the order of 1 m s^{-1} occur when synoptic wind fields are created from irregularly spaced QuikSCAT swath data. To minimize this error, they had to average the swath data over 1 degree and 2 days. Hence, gridded data sets are generally designed to trade off point-to-point accuracy in order to preserve and display the large-scale properties of the wind field.

The gridded near-real-time data we used are produced by an objective analysis of a special quickly generated set of swath data. To be useful in operational weather forecasting, data must be available within three hours after the satellite passes any location. To meet this need, a near-real-time swath data set is generated. For the sake of speed, this data set is produced from backscatter measurements with minimal time devoted to geophysical processing. Winds are retrieved using the same algorithm as the Level 2B swath data, but employ only averaged backscatter measurements instead of the more precise slice measurements. Also, a numerical weather forecast product is used to prime the ambiguity removal algorithm. To create the final gridded data set, a successive correction technique is used to interpolate the swath data onto a 0.5-degree grid once every 12 hours.

The gridded science data set is produced using the same objective analysis technique as above (Tang and Liu 1996), except the input data are from the more highly processed Level 2B swath data. More sophisticated space, time, and ambiguity algorithms are used, and rain contaminated cells are removed.

2. Buoys

The 12 near-shore buoys used in our comparisons ranged from 8 to 41 km off the US west coast, and were separated by 100 to 200 km north-south. The three offshore buoys were approximately 500 km offshore, and separated by about 400 km north-south. Most buoys had anemometers 5 m above the sea surface, but one (46023) had a 10 m anemometer. The buoys transmit wind speed and direction each hour based on an eight-minute scalar average from minute 42 to minute 50. Tests by Hamilton (1980) and Gilhousen (1987) showed the buoys have rms wind errors of 1.0 m s^{-1} and 10 degrees.

3. Matching Observations

Using the times and positions contained in the swath data, our first task was to select a single satellite observation matching each buoy observation. Since the area observed by the satellite is constantly moving, time and space tolerance intervals were necessary in order to gather reasonable numbers of comparisons. Any interval, however, potentially introduces errors, especially in variable near-shore winds, because the satellite and buoy will not be recording at exactly the same time and place. These interval-related

errors only arise in comparison studies, however, since satellite-derived wind observations are normally used when and where they are measured.

Many different tolerance intervals have been tried in satellite-buoy comparison studies (Ebuchi et al. 2002, 25 km-30 min; Freilich and Dunbar 1999, 50 km-30 min; Atlas et al. 1999, 100 km-90 min). Since 12 of the buoys we used were within the variable near-shore wind field, we selected a 25 km space tolerance that allowed reasonable numbers of satellite-buoy matches. Since the near-shore buoys were located at the very edge of the satellite's land-contaminated view, we ended up with the offshore-skewed tolerance intervals shown in Figure 3.

The time-tolerance interval for the comparisons was determined by how closely the twice-daily satellite over-flights matched the hourly buoy readings. The satellite-buoy mean time separation was only 16 minutes for the swath data at all 15 buoys. The correlation coefficients shown in Table 1 show a high level of agreement between the satellite and buoy wind speed measurements using the above time and space intervals.

Both gridded data sets were already provided on a 0.5-degree grid at 0000 and 1200 UTC. Our comparisons for the gridded data sets were done by simply selecting a wind value at the closest grid point to each buoy for both of the gridded satellite data sets. Hence the space interval was always less than 30 km.

To match the analysis time for the gridded data sets, we decided to vector average the buoy winds values over four-hour intervals centered on 0000 and 1200 UTC. A four-hour average was used in an attempt to match the smoothing applied by the objective analysis used to produce the gridded data. The satellite observations that contribute the most to the objective analysis are typically within two hours of verification time off the US west coast.

4. Corrections

For all three data sets, two wind speed corrections were considered. The first was for stability. Satellite wind data are based on neutral stability, whereas buoys measure winds in whatever stability exists locally. Mears et al.'s (2001) 11-year study at 60 buoy locations found that stability differences introduce wind speed errors of only about 0.1 m s^{-1}. Also, their range of stability conditions covered the entire range we encountered.

Since the expected errors associated with stability differences were a small percentage of the minimal wind speed used in this study (3 m s^{-1}), we neglected stability errors.

The second correction was for anemometer height. The satellite is purported to provide wind observations at 10 m above the ocean surface, whereas most of the buoys we used measured winds at 5 m. To adjust the buoy-derived wind to 10 m, we followed Smith's (1988) method. The corrections amounted to about a 7% increase in all buoy wind speeds measured at 5 m heights.

After the corrections were applied, buoy-derived wind speed and direction were subtracted from the closest matching satellite-derived wind speed and direction. This was repeated for all three satellite data sets. Although the satellite flew over the US west coast twice a day during our year and a half observation period, each pass did not cover every buoy location. Hence, we were only able to obtain several hundred comparisons within our space and time tolerances at each buoy location. Comparisons at the 12 near-shore buoys were then combined to estimate overall satellite-buoy agreement for the entire coastal zone for all seasons. The three offshore buoys were combined in similar fashion to provide a reference for comparison with the near-shore data.

5. Swath Data Tests

The first tests were done on the swath data. Since the satellite's operational range is 3 to 30 m s^{-1}, all data where buoys recorded winds less than 3 m s^{-1} were discarded. Next, rain-flagged data were removed. When overall satellite-buoy differences with and without rain were compared, there was very little difference because so little rain occurred during the test period.

After rain removal, we then studied the effects of light winds on swath data. Freilich and Dunbar (1999) showed that NSCAT satellite data contained random component errors that resulted in large direction errors at low wind speeds. They also showed that these large direction errors were greatly reduced at wind speeds greater than 6 m s^{-1}. Following their lead, we removed all observations where buoys recorded wind speeds less than 6 m s^{-1}. This editing produced a major reduction in satellite-buoy direction differences, but no reduction in speed differences.

6. Gridded Data Tests

The next comparisons were with the two gridded data sets. These sets use swath data as their source, but are produced only after the swath data has undergone extensive objective analysis and smoothing. The results are provided on a 0.5-degree grid at 0000 and 1200 UTC. There are two main differences between these two gridded data sets. The gridded near-real-time data has rain left in, and it uses the less sophisticated near-real-time swath data processing scheme.

To obtain comparable wind observations, we smoothed the buoy winds by using four-hour vector averages. These averages were centered on 0000 and 1200 UTC to match the gridded data set times. Next, each buoy wind average was subtracted from the wind value at the closest grid point in the gridded data set. Finally, we combined all the near-shore differences over the entire observation period for the 12 coastal buoys, and did the same for the 3 offshore buoys. This entire process was repeated for both the gridded near-real-time and the gridded science data sets.

C. RESULTS

1. Near-Shore Swath Data

Figure 5 shows box plots of satellite-buoy wind differences for the swath data at each near-shore buoy. There are considerable buoy-to-buoy differences. The mean speed difference varied from 0.0 to 2.0 m s^{-1}, and the mean direction difference varied from 1 degree counterclockwise to 17 degrees clockwise. Our calculations showed that these buoy-to-buoy variations were not significantly correlated with latitude, longitude, coastal topography, distance from shore, or satellite-buoy separation distance.

The combined swath data differences for all 12 near-shore buoy locations are shown in Figure 6. The distribution of speed differences is fairly normal, but the direction distribution is not normal due to some very large errors. The mean speed difference is 0.5 m s^{-1}, and the mean direction difference is 9 degrees clockwise. In order to calculate the combined rms value for all 12 buoys, we employed a pooled variance technique. This technique is used when data samples have similar variances but dissimilar means (Dixon and Massey 1969). Using this technique, the combined near-shore rms speed value was 1.6 m s^{-1} and the rms direction value was 38 degrees.

Removing rain from the swath data had little overall effect because less than ten percent of satellite-derived winds had rain flags during our test period. The rms values only decreased from 1.6 to 1.4 m s^{-1}, and from 38 to 37 degrees. Nevertheless, removing rain eliminated some instances where the satellite had much higher wind speed values than the buoy recorded, so it is an important editing tool.

In contrast to the minor effect of discarding rain-flagged observations, removing buoy wind speed values between 3 and 6 m s^{-1} had a major effect by eliminating most large direction differences. Figure 7 shows error histograms for swath data with both rain and winds less than 6 m s^{-1} removed. Speed differences have not changed much, but direction differences are both smaller and closer to a normal distribution. The rms values at all 12 near-shore buoys with both rain and winds less than 6 m s^{-1} removed, dropped from the unedited values of 1.6 m s^{-1} and 38 degrees down to 1.3 m s^{-1} and 26 degrees.

2. Near Shore Gridded Data

The gridded near-real-time data set initially incorporates all satellite data into the analysis, including observations in light winds and rain. These error-prone measurements could not be removed from our comparisons, since they have already been smoothed into surrounding points through the objective analysis scheme. Nevertheless, we attempted to partially discard light winds by removing all comparisons that had four-hour averaged buoy wind speeds less than 6 m s^{-1}. The rms differences after this editing were 3.2 m s^{-1} and 45 degrees, which are considerably larger than the swath comparisons.

The gridded science data set has rain removed before analysis, and uses a more sophisticated ambiguity removal algorithm, so theoretically it should better match the buoys than the gridded near-real-time data. Once again, we removed all comparisons where the buoy 4-hour wind speed average was less than 6 m s^{-1}. The results indicated that large direction differences, especially in the clockwise direction, were still a major source of error. These large differences are most likely due to bad directions recorded in light winds that have been incorporated into the analysis. The rms differences for the gridded science data set were 3.1 m s^{-1} and 41 degrees, only slightly smaller than the gridded near-real-time data set. Apparently, improvements in gridded science data due to rain removal, and to the more sophisticated swath processing are overwhelmed by the effects of the objective analysis on observations scattered in both space and time.

3. Offshore Comparisons

We also combined satellite-buoy differences at the three offshore buoys. With rain and winds less than 6 m s^{-1} removed, offshore swath data differences, shown in Figure 8, were more normally distributed and had considerably smaller rms values than those near shore. The overall mean speed difference was 0.2 m s^{-1} and the mean direction difference was 8 degrees clockwise. The rms values dropped from 1.3 m s^{-1} and 26 degrees near shore, to 1.0 m s^{-1} and 15 degrees offshore. These values are similar to offshore buoy comparisons from QuikSCAT done by Ebuchi et al., 2002 (1.0 m s^{-1}; and 20 degrees) and from NSCAT done by Freilich and Dunbar, 1999 (1.3 m s^{-1}; and 17 degrees).

Both gridded data sets also have lower errors offshore than near-shore. The offshore rms values for the near-real-time gridded data dropped from 3.2 m s^{-1} and 45 degrees, to 2.7 m s^{-1} and 42 degrees. The differences in the gridded science data went from 3.1 m s^{-1} and 41 degrees, to 2.5 m s^{-1} and 41 degrees.

We initially assumed the higher swath data differences near shore resulted mainly from the seaward bias of the satellite-buoy comparison areas (shown in Figure 3). These skewed areas resulted in somewhat larger satellite-buoy separation near-shore (13 km mean near-shore, 10 km mean offshore). Since many investigators (Bakun and Nelson 1991; Beardsley et al. 1987; Huyer and Kosro 1987) have shown wind speeds increasing with distance from shore, we expected this bias might account for much of the difference between offshore and near-shore comparisons.

Our attempt to verify the above effect was unsuccessful, however. Regression analyses of wind speed difference versus separation distance at each of the 12 near-shore buoys showed no consistent increase of wind speed difference with increasing satellite-buoy separation. At some locations, satellite and buoy wind speed data actually matched better with increasing separation. This regression analysis led us to conclude that satellite-buoy separation could not account for all of our observed near-shore to offshore differences.

Our next attempt to explain the difference between offshore and near-shore comparisons involved examining the wind's spectral characteristics using hourly buoy wind data. We found that the winds at the 12 near-shore buoys had large amounts of

diurnal energy, as well as other high frequencies, compared to those offshore. We also found that the strength of near-shore diurnal energy varied significantly from buoy to buoy, even at locations within 100 km of each other. Since in general, high frequency atmospheric phenomena have smaller spatial scales, the increased high frequency energy we found at the near-shore locations in conjunction with the satellite's spatial averaging may have resulted in the larger near-shore satellite-buoy differences.

4. Confidence Limits

We used standard-error calculations (Dixon and Massey 1969) to estimate confidence limits for satellite-buoy differences. These calculations use the time and space wind-correlation scales to estimate degrees of freedom. The effect is equivalent to reducing the number of observations used for calculating confidence limits. For the North American west coast, these scales are typically a few days and several hundred kilometers (Halliwell and Allen, 1987).

In our case, however, we were not dealing with wind observations directly, but rather with wind differences measured by two independent systems. Based on auto-correlations of the satellite-buoy differences, we found wind-difference correlation time scales to be less than a day, and alongshore space scales to be between 100 and 300 km. Using these values, we ended up with 1663 degrees of freedom for the 5741 swath observations. Table 2 is a summary of all statistics, including confidence limits, for the near-shore and offshore swath data.

D. DISCUSSION

Based on our comparisons of three QuikSCAT data sets (swath, gridded near-real-time, and gridded science data), swath data provide the best agreement with near-shore buoy wind data. This was as expected since gridded data sets are not designed to provide point-to-point accuracy, but rather to depict large-scale wind patterns. All three data sets, however, contain two types of errors near shore.

The first type consisted of large wind direction errors. In addition to the numerous direction errors recorded by the satellite in light winds, we occasionally found large errors at higher wind speeds. These errant wind directions typically occurred for a single satellite observation, and with a frequency of about one observation in 50. Although these

direction errors were usually possible to identify in our large statistical samples, they would not be easy to discern in operational applications. We suspect that these large direction errors are due to improper ambiguity removal in the satellite data processing scheme. Near shore, the effectiveness of the ambiguity removal process is limited by two factors. First, the numerical weather product used in the nudging process has just a one-degree resolution in complex near shore winds. Second, the modified median filter is hampered by the lack of wind vector cells on the shore side.

Other wind direction ambiguity removal algorithms are available. For example, the Direction Interval Retrieval with Threshold Nudging (DIRTH) algorithms make greater use of spatial information in determining the wind vector, but, as a result, are more likely to smooth small-scale near-shore features (Stiles et al. 2002).

As a result of the above difficulties in the currently available direction algorithms, the best procedure at present for improving QuikSCAT near-shore wind directions seems to be editing. Removing light winds greatly reduces the number of large direction errors. Also, time series plots of wind direction could be used to highlight single-point spikes that may be reduced or removed using techniques such as averaging or band pass filtering. Such editing can also be used to remove direction biases such as the clockwise offset we found at eleven of the twelve near shore buoys and all offshore buoys.

The second type of error consisted of large wind speed spikes. QuikSCAT wind speeds are known to be erratic in rain, but even after we removed rain-flagged cells, some large single-point wind speed errors remained. We discovered that by decreasing the thresholds in the rain-flagging algorithm, most of these large errors could be removed. Unfortunately, this technique also removed some surrounding good data as well. Apparently the satellite's rain flag is somewhat less effective near shore where the algorithm is hampered by the lack of comparison cells on the shore side.

These large speed errors were few in number in our study because there was little rain in the area during our test period. In near-shore regions with moderate to heavy rain, however, either a more effective rain flag, or a wind-retrieval algorithm capable of making wind estimates in rain is necessary.

Even after our low wind speed and rain editing of the swath data, there were still large differences between offshore and near-shore satellite-buoy comparisons. At near-shore buoys, satellite-buoy speed differences were about 30% larger, and direction differences were about 70% larger than at offshore buoys. Since the gridded data sets are derived from swath data, they showed the same pattern of differences. Our conclusion is that these differences were mainly due to the complexity of the coastal winds. Spectral analysis showed winds at the near-shore buoys had more high-frequency energy, and more buoy-to-buoy variability than those at the offshore buoys. Others have observed this as well. For example, Beardsley et al. (1987) and Winant et al. (1987) measured nearly a 3-fold increase in wind speed, and a 30-degree direction change within the first 30 km off northern California. In such complex wind fields the satellite's 25 km space average will interject smoothing errors. If this spatial averaging is the primary source of the larger near-shore errors, then a higher spatial resolution technique will reduce this problem but may increase other errors.

Gridded data are designed to depict large-scale meteorological features, and are not designed for the point-to-point comparisons we did. The two JPL gridded products we tested suffered for two reasons. First, aliasing is introduced by the satellite's 12-hour sampling rate, and its constantly migrating track. Second, the observations include large wind direction errors due to light winds. Consequently, we expected satellite-buoy differences to be larger in the gridded data sets than in the swath data.

Nevertheless, all three data sets would benefit from certain improvements. More precise methods for ambiguity removal and better rain flagging would increase satellite wind accuracy everywhere. Also, increased spatial resolution would improve near-shore accuracy. And finally, the increased sampling provided by a second satellite scatterometer would improve swath coverage and reduce aliasing in the gridded data sets.

Even with the present QuikSCAT system, however, we found the agreement between such vastly different wind-observing systems as satellites and buoys remarkable. Our overall estimate of near-shore satellite-buoy rms differences in swath data (1.3 m s^{-1} and 26 degrees) was within the satellite's design specifications for wind speed (+/- 2 m s^{-1}), and close to the design specification for direction (+/- 20 degrees). Moreover, the

above comparisons include the errors occurring in buoy data (1 m s^{-1} and 10 degrees) as well as errors from our inexact time and space matches.

The results of this study show that the QuikSCAT Level 2B swath data are accurate enough for our planned use in identifying strong upwelling episodes. These satellite wind data will be particularly useful in the many coastal areas of the world's oceans that currently lack in situ wind measurements. However, the near-shore wind data is only marginally useful in light winds because of the satellite's decreased ability to determine wind direction under those conditions. Finally, we believe that the QuikSCAT Level 2B swath data, with modest post-processing, are sufficiently accurate for many coastal studies.

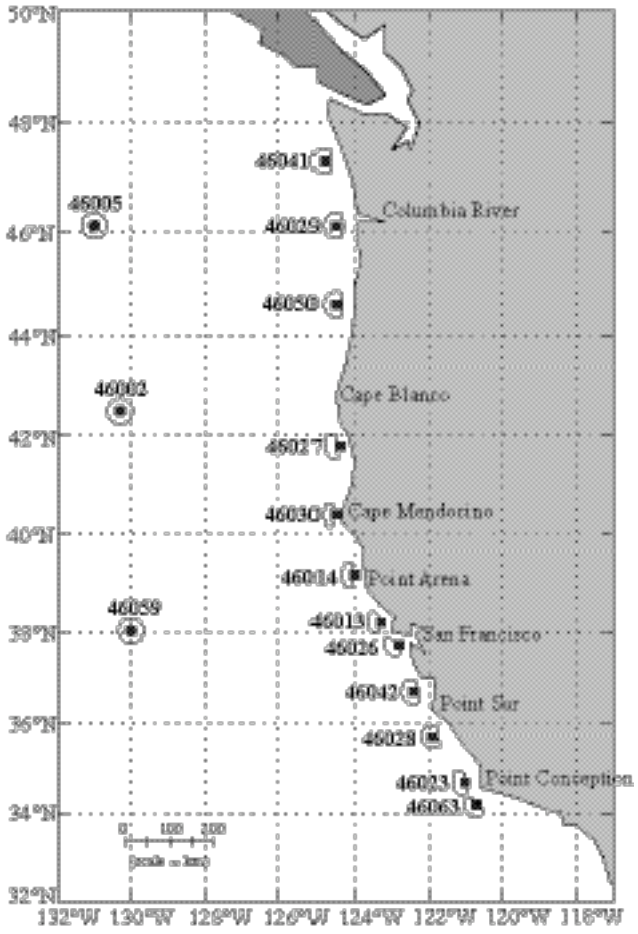

Figure 3. Locations of 12 near shore buoys (marked with squares), and three offshore buoys (circles) used to evaluate QuikSCAT satellite wind observations. Marked areas around buoys indicate the maximum allowed spatial separation of satellite and buoy observations used for comparisons.

Table 1. Properties of the data set used to compare QuikSCAT swath and buoy wind data. Separation distances are the average distance between the center of the satellite's wind observation area and the buoy's location.

Near-Shore Buoys	Position (lat, lon)	Distance from shore (km)	Number of matching pairs	Average separation distance (km)	Correlation (speed)
Buoy 46041	47.3N, 124.8W	34	554	9	0.9
Buoy 46029	46.1N, 124.5W	36	486	9	0.9
Buoy 46050	44.6N, 124.5W	35	563	10	0.9
Buoy 46027	41.8N, 124.4W	13	198	22	0.8
Buoy 46030	40.4N, 124.5W	8	252	22	0.9
Buoy 46014	39.2N, 124.0W	17	485	17	0.8
Buoy 46013	38.2N, 123.3W	22	591	14	0.9
Buoy 46026	37.7N, 122.8W	20	496	17	0.8
Buoy 46042	36.7N, 122.4W	35	562	9	0.9
Buoy 46028	35.7N, 121.9W	41	354	10	0.9
Buoy 46023	34.7N, 121.0W	31	628	9	0.9
Buoy 46063	34.2N, 120.7W	30	572	13	0.9
		mean= 27 km	total obs= 5741	mean= 13 km	
Offshore Buoys					
Buoy 46005	46.1N, 131.0W	545	704	10	0.9
Buoy 46002	42.5N, 130.3W	475	420	10	0.9
Buoy 46059	38.0N, 130.0W	540	796	10	0.9
		mean= 520 km	total obs= 1920	mean= 10 km	

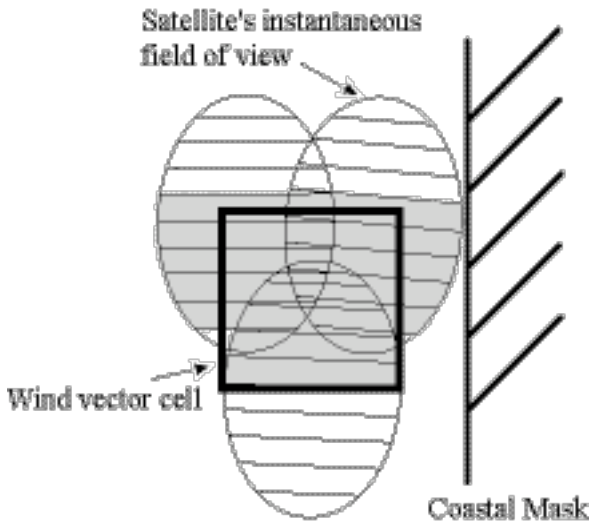

Figure 4. Simplified schematic showing backscatter measurements from the QuikSCAT satellite. As the satellite's field of view (elliptical area) sweeps across the satellite's path, current and previous fields-of-view overlap. These fields are divided into slices, which are then combined to create 25-km wind vector cells. If any slice is determined to be within the coastal mask, the entire wind vector cell is flagged as contaminated.

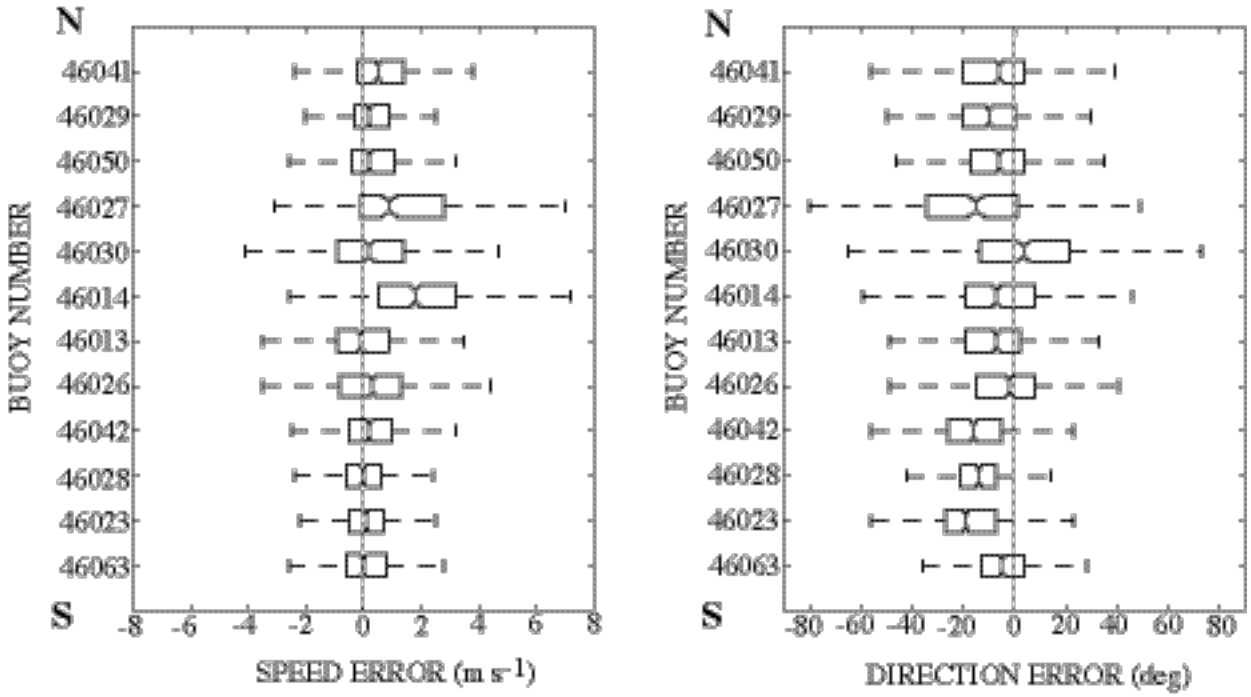

Figure 5. Distributions of differences between QuikSCAT swath and near-shore buoy wind data. Speed differences for all 12 near-shore buoys are shown in the left figure; direction differences in the right figure. Each box shows the 25th, 50th, and 75th distribution percentiles. Dotted lines show the rest of the distribution excluding outlying points (greater than 1.5 times the inter-quartile range). Notches in boxes represent confidence intervals about the 50th percentile.

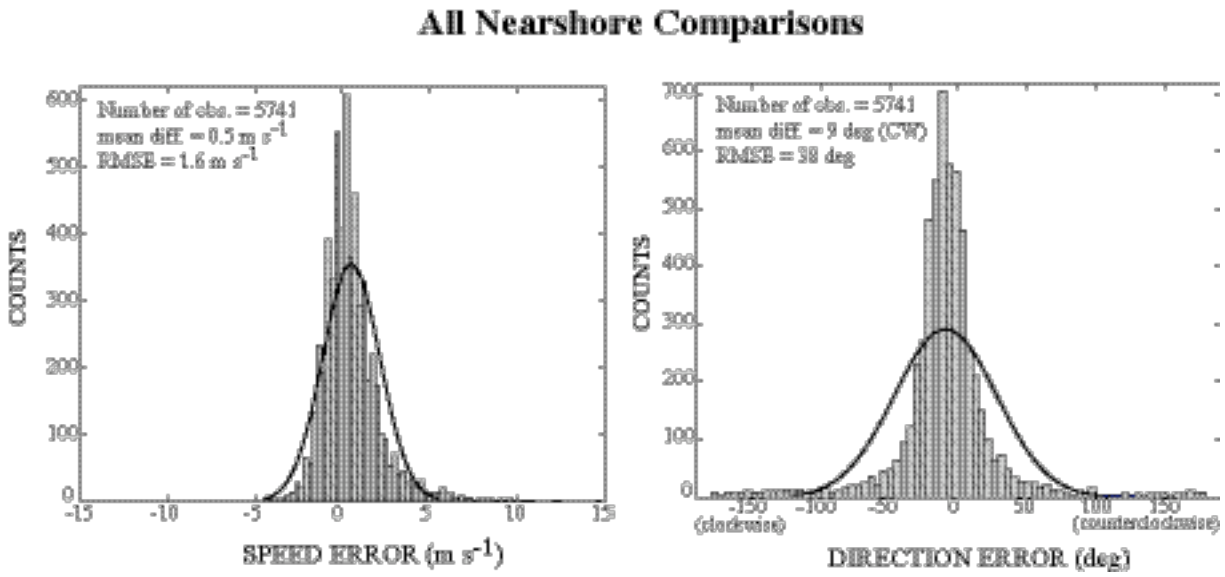

Figure 6. Cumulative histograms of wind differences between QuikSCAT swath data and near-shore buoys. Speed differences for all 12 near-shore buoys are grouped in the left figure, and direction differences in the right figure. Solid curves are normal distributions. Winds less than 3 m s-1 have been removed; rain has not. Speed differences are approximately normally distributed but have a grouping of large errors on the right side of the histogram. Direction differences, however, are not normally distributed due to the large errors on both sides of the histogram.

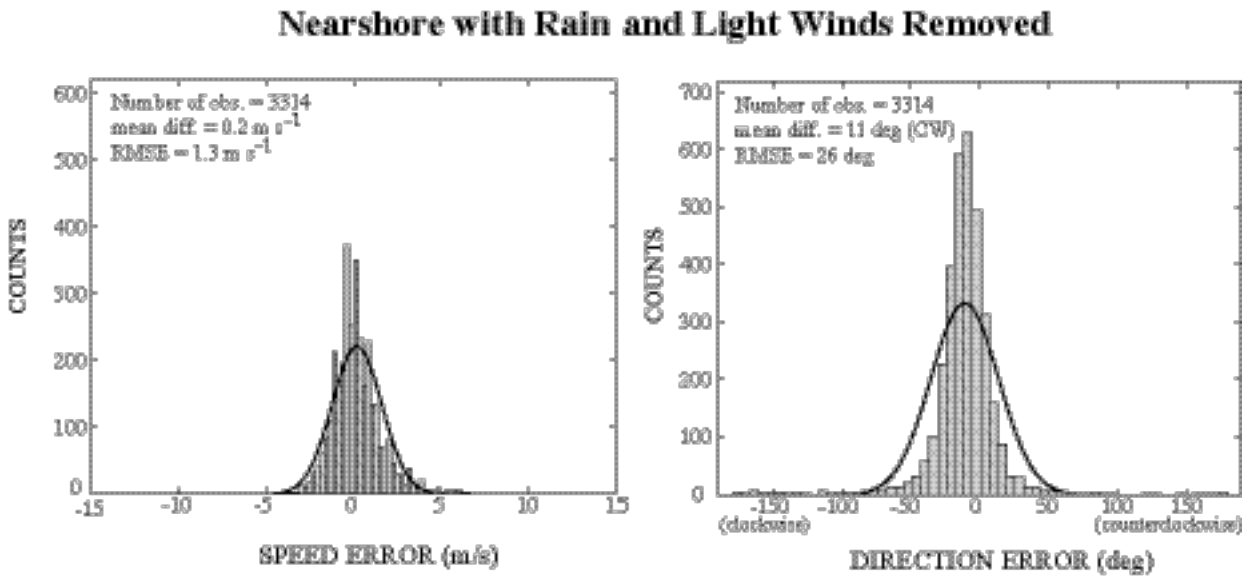

Figure 7. Cumulative histograms of edited wind differences between QuikSCAT swath data and near-shore buoys with rain-flagged observations and winds less than 6 m s^{-1} removed. Both speed and direction differences are more normally distributed.

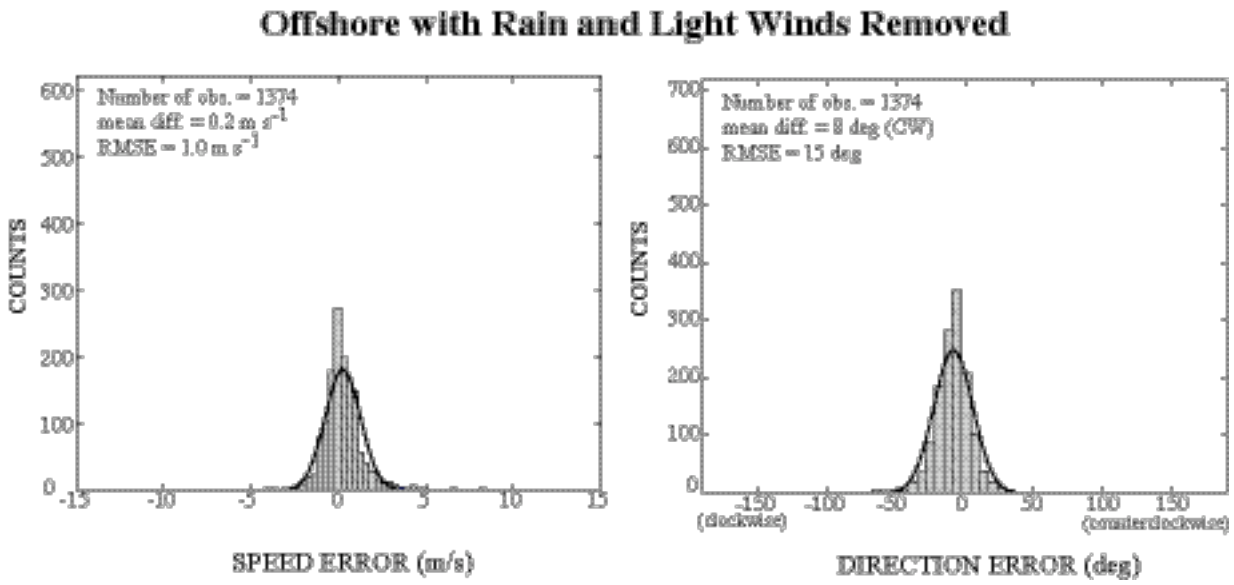

Figure 8. Cumulative histograms of edited wind differences between QuikSCAT swath data and offshore buoys with rain flagged observations and winds less than 6 m s^{-1} removed. Both wind speed and direction differences are approximately normally distributed.

Table 2. Summary of differences between QuikSCAT satellite swath data and buoy wind data.

QuikSCAT Data	Editing	Number of Observations	Mean Error Speed (m/s)	Direction (deg clockwise)	RMS Error Speed (m/s)	Direction (deg)
Near-shore						
Swath	Rain in, winds < 3 m/s out	5741	0.5 (+/- .1)	9 (+/- 2)	**1.6 (+/- .1)**	**38 (+/- 3)**
Swath	Rain out, winds < 3 m/s out	5241	0.4 (+/- .1)	9 (+/- 2)	**1.4 (+/- .1)**	**37 (+/- 3)**
Swath	Rain out, winds < 6 m/s out	3314	0.2 (+/- .1)	11 (+/- 2)	**1.3 (+/- .1)**	**26 (+/- 2)**
Offshore						
Swath	Rain out, winds < 3 m/s out	1895	0.2 (+/- .1)	8 (+/- 1)	**1.0 (+/- .1)**	**20 (+/- 1)**
Swath	Rain out, winds < 6 m/s out	1374	0.2 (+/- .1)	8 (+/- 1)	**1.0 (+/- .1)**	**15 (+/- 1)**

THIS PAGE INTENTIONALLY LEFT BLANK

III. ESTIMATING UPWELLING OFF THE WEST COASTS OF NORTH AND SOUTH AMERICA

A. INTRODUCTION

Marine ecosystems off the west coasts of North and South America, sustained by coastal upwelling, account for approximately one fifth of the world's total marine fish catch (Food and Agriculture Organization of the United Nations, 1995). The dominant commercial species include anchovy (*Engraulis mordax, E. ringens*), jack mackerel (*Trachurus murphyi*), chub mackerel (*Scomber japonicus*), and sardine (*Sardinops sagax*). From 1994 to 1998 the average annual catch in these regions was 8 million metric-tons of anchovy, 4 million metric-tons of jack mackerel, 2 million metric-tons of chub mackerel, and 1 million metric-tons of sardine. In addition, the prevalence of these smaller species attracts commercially important predators such as tuna (*Thunnus spp., Euthynnus pelamis*), swordfish (*Xiphias gladius*), and salmon (*Oncorhynchus spp*.). These larger fish also attract sport fishing which provides significant local economic impact.

The National Oceanic and Atmospheric Administration's (NOAA) Pacific Fisheries Environmental Laboratory (PFEL) routinely disseminates monthly upwelling estimates at sites off the west coasts of North America and South America (Schwing et al., 1996; Norton et al., 2001). The purpose of these estimates, called upwelling indices, is to highlight places and times of potentially high biological productivity associated with coastal upwelling. The North American sites range from 21°N (off Cabo San Lucas in Baja, California) to 60°N (off the Kenai Peninsula in Alaska), and span the entire California Current system (Figure 1). The South American sites are between 15°S (near Lima, Peru) and 45°S (off southern Chile), and are within the Peru-Chile current system (Figure 2). The North American upwelling indices have been available since 1946, and the South American since 1981.

Although the upwelling estimations involve a host of assumptions and approximations, they are nevertheless widely used. They have been referenced in over 400 fisheries publications (e.g., Brodeur and Ware, 1992; McConnaughey et al., 1992; Ainley et al., 1995; Parrish and Mallicoate, 1995; Borja et al., 2002; Koslow et al., 2002;

Mueter et al., 2002). Moreover, they are the only regularly produced coastal upwelling estimates and have been produced by the same method since inception. As a result, they provide a consistent, long-term reference for relating environmental variability to biological time series such as fish catch.

Many studies have attempted to correlate upwelling with fisheries productivity. Recent studies (Gargett, 1997; Ryding and Skalski, 1999; Botsford et al., 2003; Stenevik, et al., 2003), however, have indicated that such correlations are weak because relationships between upwelling and productivity are not necessarily linear. Cury and Roy (1989), for example, showed that maximum reproductive success of several species occurs only in moderate upwelling. For such species upwelling estimates need to be precise.

To improve the estimates of upwelling, PFEL updated its technique in 2001 (http://las.pfeg.noaa.gov/las/main.pl, click the "i" icons for information on each product). The Bakun (1973) method is still used, but higher resolution pressure fields, a variable drag coefficient (Trenberth et al., 1990), and winds from U.S. Navy Operational Global Atmospheric Prediction System (NOGAPS; Hogan and Rosmond, 1991) are now available. Users can tailor these enhancements to suit their needs and estimate upwelling in any ocean location at any time.

Since a model-derived wind option is now available, we decided to test it to see if it provided better upwelling estimates than the historic geostrophic method. To do this, we compared upwelling estimates based on geostrophic and on model-derived winds to a reference based on satellite-measured winds at 14 North American and 11 South American sites from August 1999 to December 2001. Our results indicate that Navy model-derived winds result in better upwelling estimates at more locations than those based on geostrophic winds.

B. METHODS

1. Satellite-Measured Winds

The polar-orbiting QuikSCAT satellite provides a space-averaged wind measurement over each 25 km ocean area. Measurements at each location occur approximately every 12 hours as the satellite passes overhead. The measurements are available from several agencies in different formats. The set used here (referred to by

NASA as Level 2B swath data; Jet Propulsion Laboratory, 2001) has been shown to be the most accurate (Pickett et al., 2003). Due to inherent limitations of the satellite's sensor, we excluded satellite wind measurements recorded within 25 km of shore, in rain, and in winds less than 3 m s^{-1}. Finally, we corrected for a nine-degree clockwise bias in the wind-direction (Pickett et al., 2003). The satellite winds were then verified with 15 U.S. west coast NOAA weather buoys. Results showed that over the period August 1999 to December 2001 weekly averaged, satellite wind components matched those recorded at the buoys within 1.6 m s^{-1} rms near-shore, and 0.8 m s^{-1} rms offshore.

2. Geostrophic-Derived Winds

The present PFEL geostrophic method uses six-hourly, one-degree surface pressure data from the U.S. Navy's NOGAPS model. The numerical model uses the equations of motion formulated in spherical coordinates with a hybrid vertical coordinate (Hogan and Rosmond, 1991). The dynamics formulation uses vorticity, divergence, virtual potential temperature, specific humidity, and terrain pressure. Observations from ships, buoys, aircraft, and satellites are assimilated into the model on a daily basis. The QuikSCAT data described above is not currently assimilated into the model. East-west and north-south pressure gradients extracted from the surface level of this model are used to estimate geostrophic winds. To account for friction, the geostrophic winds are rotated 15 degrees (counterclockwise in the northern hemisphere; clockwise in the southern) and their speed reduced by 30% (Fofonoff, 1962).

For this study, the above procedure was used to provide the geostrophic winds that were compared to satellite-measured winds. We matched the six-hourly geostrophic winds to satellite measurements that were within three hours and 25 km of each North and South American test site. The components of the geostrophic and satellite-based winds were then weekly averaged and compared at the 25 sites (locations in Figures 1 and 2; site properties in Table 3). Comparisons from August 1999 to December 2001 resulted in 127 pairs of weekly averaged wind-components at each site.

3. Model-Derived Winds

We tested surface winds extracted from the NOGAPS model in a similar fashion. Since the Navy only archived model output at 0000 and 1200 UTC, we selected satellite wind measurements that were within three hours of these times and within 25 km of each

site. Having access to only two model outputs per day did not significantly reduce the number of matching observations because the satellite passed over the test sites close to these times. It did, however, mean that the matching satellite measurements were slightly different than they were for the geostrophic winds. The 12-hourly model and satellite wind components were then weekly averaged and compared for the same period of August 1999 to December 2001.

4. Upwelling Estimates

The above three sets of wind data were next used to estimate three comparable sets of upwelling data. To compute upwelling based on geostrophic winds, we used the traditional Bakun (1973) method. All wind components were converted to wind-stress, τ, using the bulk formula (Gill, 1982):

$$\tau = \rho_a C_d |\boldsymbol{v}| \boldsymbol{v} \qquad \text{(units = N m}^{-2}\text{)}$$

where ρ_a is the density of air (1.2 kg m^{-3}), C_d a constant drag coefficient (.0013), and $\boldsymbol{v}$ the wind vector with magnitude $|\boldsymbol{v}|$. These stress components were then used to estimate offshore Ekman transport, **M** (Smith, 1968; Bakun, 1973):

$$\mathbf{M} = \frac{1}{\rho_w f} \tau \times \mathbf{k} \qquad \text{(units = m}^3\text{ s}^{-1}\text{ per 100 meters of coastline)}$$

where τ is the derived weekly averaged wind-stress vector; ρ_w the density of seawater (assumed constant at 1024 kg m^{-3}); f the Coriolis parameter; and **k** the unit vertical vector. Next, the offshore component was calculated from the dot product of the above transport vector with an orthogonal drawn to a three-degree (of latitude) segment of the local coastline. By using this same method of calculation for satellite-measured, geostrophic-derived, and model-derived winds, we ended up with three sets of weekly upwelling estimates for 127 weeks at 25 sites. The upwelling estimates based on satellite-measured winds were used as the reference to evaluate geostrophic and model-based upwelling.

We used both correlation coefficients and skill scores to gage agreement between the satellite-based upwelling and the estimates from geostrophy and the model. Skill scores provide a more demanding test of agreement between derived and measured data

than correlation does. For example, two linear data sets offset from each other by a constant would have a high correlation but a low skill score. Skill score is based on differences between test and observed data sets divided by differences between a control data set and the observed data set. The control data set is usually a random variable with the same mean and standard deviation as the observed data (Von Storch and Zwiers, 1999). If the test and observed data sets match exactly, skill score would equal one. If the differences between the test data and the observed data equaled the differences between the random variable and the observed data, skill score would be zero. If the differences between the test and observed data were larger than those of the random variable, skill score would be less than zero.

The skill score we used is called the Brier skill score (Von Storch and Zwiers, 1999), and is defined as:

$$SS = 1 - [MSE/MSE_r]$$

where *MSE* is the mean-square difference between the test data set (either geostrophic or model-based in our case) and the reference data set (satellite-based), and MSE_r is the difference between a control data set and the reference. A control set is used to normalize the mean-square error so comparisons are valid among sites with different statistical properties. Our control data set was a random variable with a mean and standard deviation matching the satellite-based upwelling at each particular site being tested. To evaluate agreement between the test and the reference upwelling data sets, we used Murphy and Epstein's (1989) criteria which requires large samples to have either correlations exceeding 0.6, or skill scores exceeding 0.2.

C. RESULTS

1. Wind Regions

Satellite wind measurements at North American sites revealed three distinct wind regions. At higher latitudes (>50°N) winds were variable, with several weeks of strong southeast winter winds that generated annual net downwelling. At middle latitudes (35°N to 45°N) winds were less variable with strong summer northwest winds that produced annual net upwelling. At lower latitudes (<35°N) winds were consistently from the northwest and generated year-round upwelling. In addition to these three regions, there

was a small, calm transition zone between the higher and mid-latitude regions (45°N to 50°N) with little upwelling or downwelling. Figure 9 shows winds at a typical site within each of the three regions. The boundaries of these regions can also be seen in the mean upwelling values listed in Tables 4 and 5. The existence, and hence consistency, of these wind regions has been confirmed by others (e.g., Parrish et al., 1981, using a compilation of surface marine observations; Halliwell and Allen, 1987, using buoys and coastal weather stations; Dorman and Winant, 1995, using buoys; and Schwing and Mendelssohn, 1997, using the Comprehensive Ocean-Atmosphere Data Set).

Winds off South America had less distinct regions, and seasonal changes were reversed. At higher latitudes (>36°S) winds were the most variable, but there were enough weeks of winds from the south to generate annual net upwelling. At middle latitudes (24°S to 36°S) strong southern winds generated large year-round upwelling. Lower latitudes (<24°S) had consistent southeast winds that also produced strong year-round upwelling. Figure 10 shows satellite winds from a sample site within each of the three regions off South America. These wind regions have also been observed in other studies (Bakun and Parrish, 1982, using a compilation of surface marine observations; Brink et al., 1983, using moorings and coastal stations off Peru; Muller and Figueroa, 1996, using ship data off Chile; Shaffer et al., 1999, using satellite data off central Chile; Blanco et al., 2001, using shore stations off northern Chile).

2. Wind Comparisons

Differences between model-derived winds and satellite-measured winds were generally smaller than those of geostrophic winds. For the entire data set (25 sites, 3,173 comparisons) model-derived winds had rms differences of 1.2 m s^{-1} for the eastward and 1.3 m s^{-1} for the northward component. Geostrophic-derived winds, on the other hand, had rms differences of 1.8 m s^{-1} for both the eastward and northward components. The model's smaller component differences appeared to stem mostly from better wind directions. The model's wind speed advantage was minor (1.7 m s^{-1} rms for model over the entire data set, 1.8 m s^{-1} rms for geostrophic) compared to its direction advantage (31 degrees rms for model, 38 degrees rms for geostrophic). Mostly as a result of better wind directions, the model provided more accurate winds than geostrophy did at 20 of the 25 sites.

Comparisons of satellite-measured, geostrophic-derived, and model-derived winds in two vastly different wind regions are shown in Figures 11 and 12. Figure 11 is an example of a middle latitude North American site (39°N, 125°W near Cape Mendocino) where agreement was fairly good. Although the summer wind patterns are similar in all three data sets, geostrophic-derived winds are slightly stronger and have a clockwise bias. Figure 12 is an example of a lower latitude South American site (15°S, 77°W off Lima, Peru) where agreement between geostrophic and measured winds was poor. At this location, geostrophic-derived winds are much stronger than either satellite-measured or model-derived winds.

3. North American Upwelling Comparisons

Next, we compared upwelling estimates derived from the three sets of wind data. Upwelling comparisons amplify wind errors since they use wind speed squared. Comparisons of upwelling estimates from satellite-measured, geostrophic-derived, and model-derived upwelling at typical higher, middle, and lower latitude North American sites are shown in Figure 13. Both geostrophic and model-derived upwelling estimates matched the satellite-derived weekly and seasonal cycles of upwelling and downwelling. Geostrophic-derived upwelling estimates had high correlations with satellite-derived estimates at all sites, and high skill scores at 12 of the 14 sites (Figure 14, Table 4). However, geostrophic-derived estimates were too high during strong upwelling and downwelling events. Also, the overall mean upwelling value was low at all North American sites (Table 4). By contrast, model-derived upwelling estimates off North America had both high correlations and skill scores at all sites (Figure 14, Table 5). In addition, the model-derived estimates had higher skill scores than geostrophic-derived estimates at most sites.

4. South American Upwelling Comparisons

Geostrophic-derived upwelling estimates did not do as well off South America. Upwelling estimates for the lower latitude sites had no meaningful correlation and no skill (Figure 15, Table 4). Model-derived upwelling estimates off South America, however, did much better. Correlations were high at all sites, and skill scores were high at 9 out of 11 sites. The only consistent problem with the model-based upwelling estimates off South America was that they had a negative bias at every site.

D. DISCUSSION

Based on our 25 sample sites, geostrophic-derived winds were reasonably accurate at most locations off North America's west coast. Off South America, however, geostrophic-derived winds had large errors, especially at lower latitudes. Why these winds were so poor at South American lower latitude sites (24°S to 15°S) is unclear. This is especially odd since Ward and Hoshkins (1996) compared open-ocean surface pressure and wind measurements to show that geostrophy worked well to within 10 degrees of the equator in both hemispheres. A likely explanation for this poor performance is the rugged adjacent coastal topography. The 6,000-meter high coastal mountains at these sites can produce both near-shore bands of strong wind-stress and wind-stress curl (Dorman et al., 1995; Dorman et al., 2000) as well as large surface pressure changes (Winant et al., 1988). The result is complex fine-scale flow and distorted near-shore surface pressure gradients.

Model-derived winds, on the other hand, agreed with measured winds better than those from geostrophy at most sites. The model uses fewer approximations and thus avoids the pitfalls inherent in geostrophic calculations. The model's full-scale dynamics allow for non-geostrophic flow induced by coastal mountains (Hogan and Rosmond, 1991; Hogan and Brody, 1993). The result was that model-based winds provided reliable upwelling estimates in more regions than did geostrophic-based winds. Upwelling estimated from model winds agreed with those from measured winds at nearly all sites off both North and South America. The only two South American sites where the model did poorly occurred just south of the Peru-Chile border, where the coastline veers sharply from north-south to east-west. Apparently the model's 100-km resolution is too coarse to track alongshore wind changes associated with abrupt topographic steering.

The best upwelling estimates, of course, would come from using measured wind stress. Polar-orbiting satellites would be a logical choice for such measurements given their global, real-time coverage. However, their migrating orbits do not allow continuous measurements. Several satellites would be required to provide complete coverage. Moreover, these expensive and complex wind-observing satellites only last a few years. The QuikSCAT satellite used for this study is already past its expected lifetime. A

replacement has been launched but data are not currently available as the satellite recently developed communication problems.

A more efficient and reliable solution would be to assimilate the satellite wind data into operational models. The Navy is planning to assimilate QuikSCAT data into their model in the near future. Once this occurs, the model's wind output should be even better.

Even with satellite data included, however, wind output from a global model will have limits for estimating upwelling. Such models lack sufficient resolution to depict small-scale topographic wind steering and wind-stress curl. Investigations with high-resolution regional models have revealed that narrow near-shore bands of strong wind-stress and wind-stress curl, missed in global models, are major contributors to regional upwelling (Pickett and Paduan, 2003). Recent improvements in the resolution of global models (to roughly 50 km in 2003) will help account for some of the upwelling produced by these small-scale features. However, a resolution of at least 10 km will be required to fully account for the topographically induced upwelling described by Pickett and Paduan (2003).

As satellite wind data are incorporated into global models and their resolution improves, more details of upwelling areas will be revealed. Such improvements will better define high-catch areas and allow improved predictions of reproductive success and future fish stocks.

In summary, our tests have shown that the 60 years of historic upwelling indices for the west coast of North America are reasonably accurate at most sites. However, by switching from geostrophic-based to the Navy's model-based winds, upwelling estimates can be confidently extended to regions were geostrophic-based upwelling estimates fail.

Table 3. Properties of upwelling sites used in this study.

North America (Lat, Lon)	**Distance to Shore** (kilometers)	**Coastal topography** (meters)
60N,146W	45	2356
57N,137W	75	1380
54N,134W	55	1194
51N,131W	110	1273
48N,125W	25	2424
45N,125W	75	1024
42N,125W	55	1368
39N,125W	110	674
36N,122W	35	1571
33N,119W	110	1736
30N,119W	275	3069
27N,116W	130	559
24N,113W	115	2164
21N,107W	150	2280
Mean	**98**	**1648**
South America		
15S, 77W	115	6425
18S, 73W	150	5806
21S, 72W	190	5974
24S, 72W	150	6750
27S, 73W	190	6080
30S, 73W	135	5430
33S, 73W	115	6959
36S, 74W	110	3830
39S, 75W	135	2840
42S, 76W	145	2290
45S, 76W	110	2290
Mean	**140**	**4970**

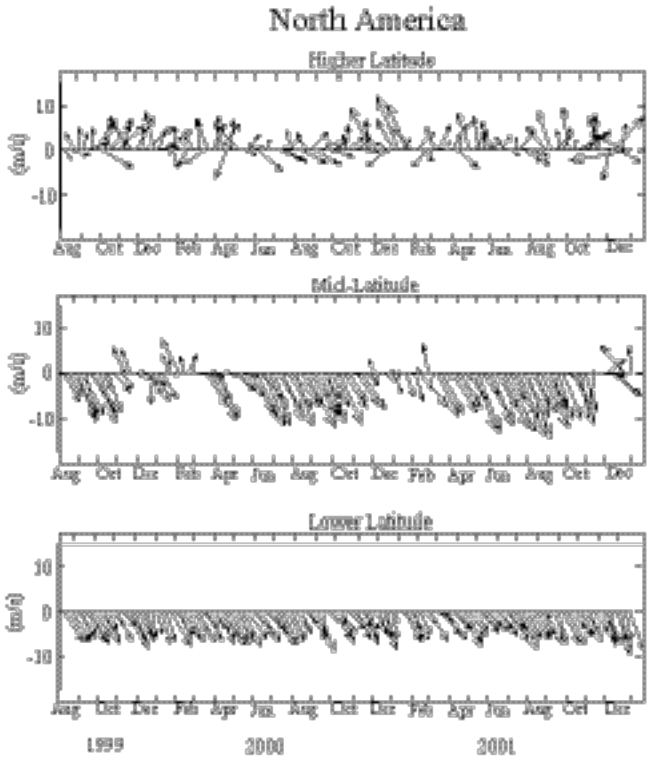

Figure 9. Measured winds at three sample sites representing higher, mid, and lower latitude regions off the North American west coast. Winds in m s^{-1} were recorded by the QuikSCAT satellite, and have been weekly averaged. The higher latitude site is 54°N, 134°W (off the Queen Charlotte Islands, British Columbia), the mid-latitude site is 39°N, 125°W (near Cape Mendocino, California), and the lower latitude site is 27°N, 116°W (off central Baja California).

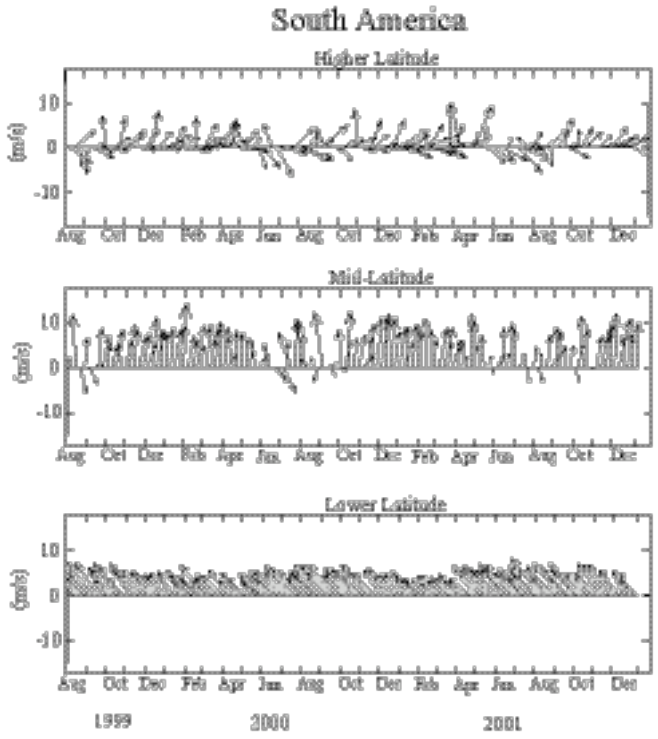

Figure 10. Measured winds at three sample sites representing higher, mid, and lower latitude regions off the South American west coast. Winds in m s^{-1} were recorded by the QuikSCAT satellite, and have been weekly averaged. The higher latitude site is 42°S, 76°W (off southern Chile), the mid-latitude site is 33°S, 73°W (near Valparaiso, Chile), and the lower latitude site is 15°S, 77°W (near Lima, Peru).

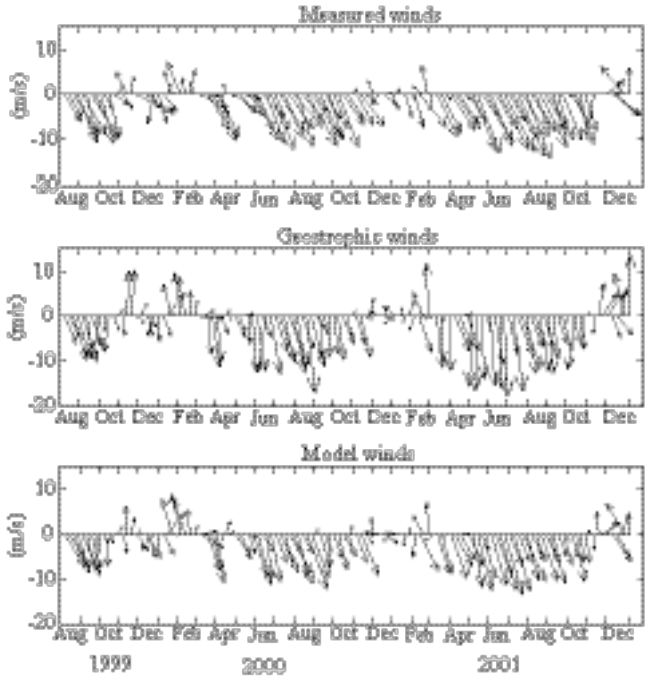

Figure 11. Comparison of satellite-measured, geostrophic-derived, and model-derived surface winds at a sample North American mid-latitude site located at 39°N, 125°W (near Cape Mendocino, California). Measured winds are from the QuikSCAT satellite and model winds are from the U.S. Navy's global atmospheric model.

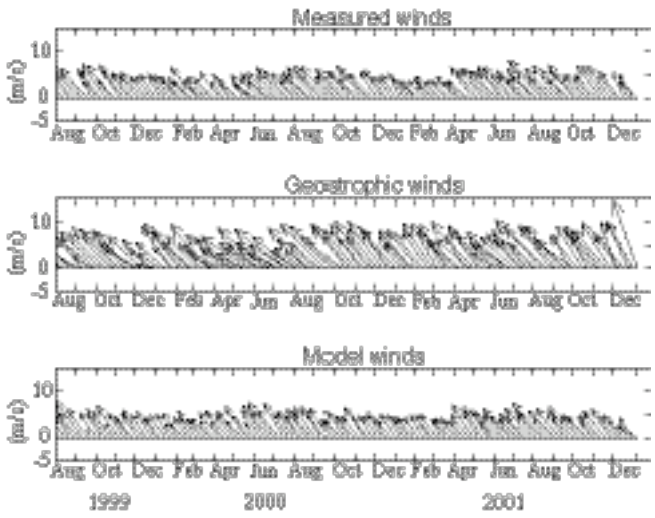

Figure 12. Comparison of satellite-measured, geostrophic-derived, and model-derived surface winds at a sample South American lower latitude site located at 15°S, 77°W (near Lima, Peru). Measured winds are from the QuikSCAT satellite and model winds are from the U.S. Navy's global atmospheric model.

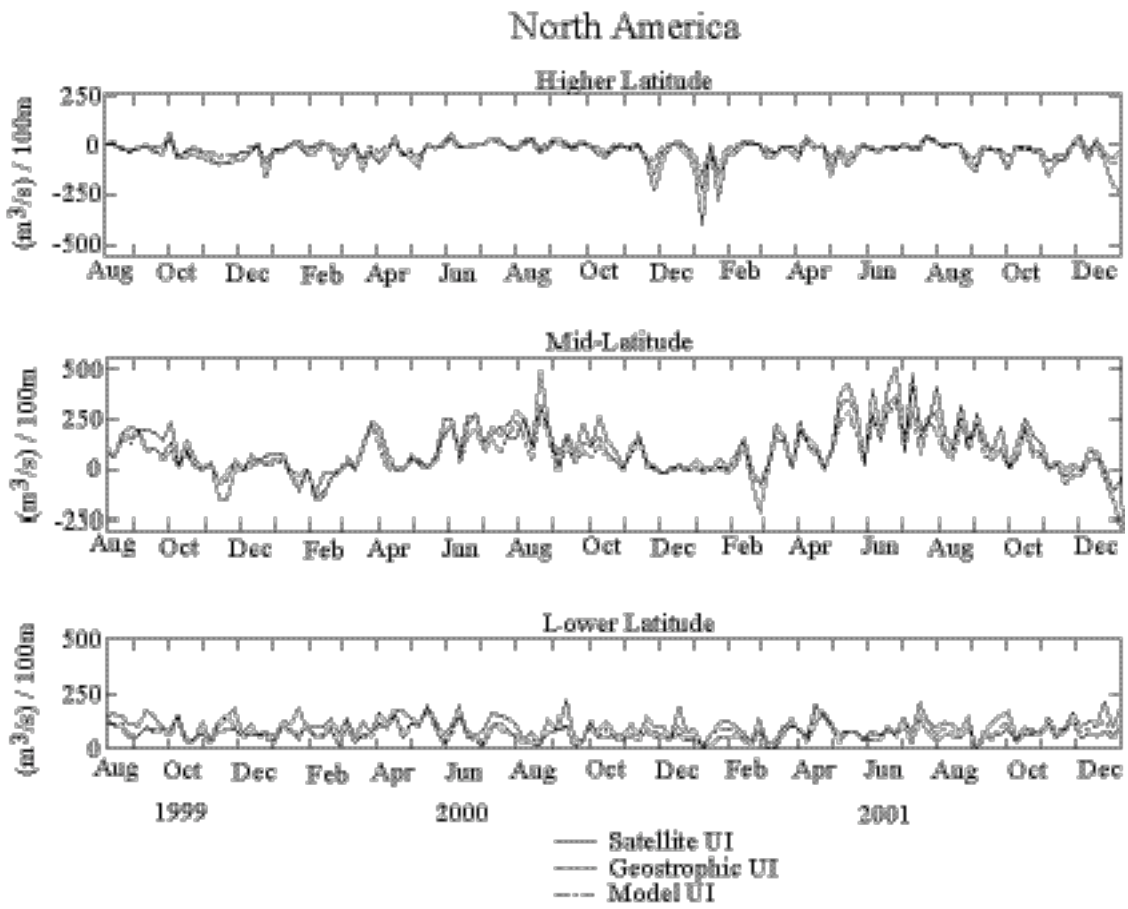

Figure 13. Upwelling estimates at three North American sites based on satellite-measured (solid line), geostrophic-derived (dashed line), and model-derived (dash-dot line) surface winds. The higher latitude site is 54°N, 134°W (off the Queen Charlotte Islands, British Colombia), the mid-latitude site is 39°N, 125°W (near Cape Mendocino, California), and the lower latitude site is 27°N, 116°W (off central Baja California).

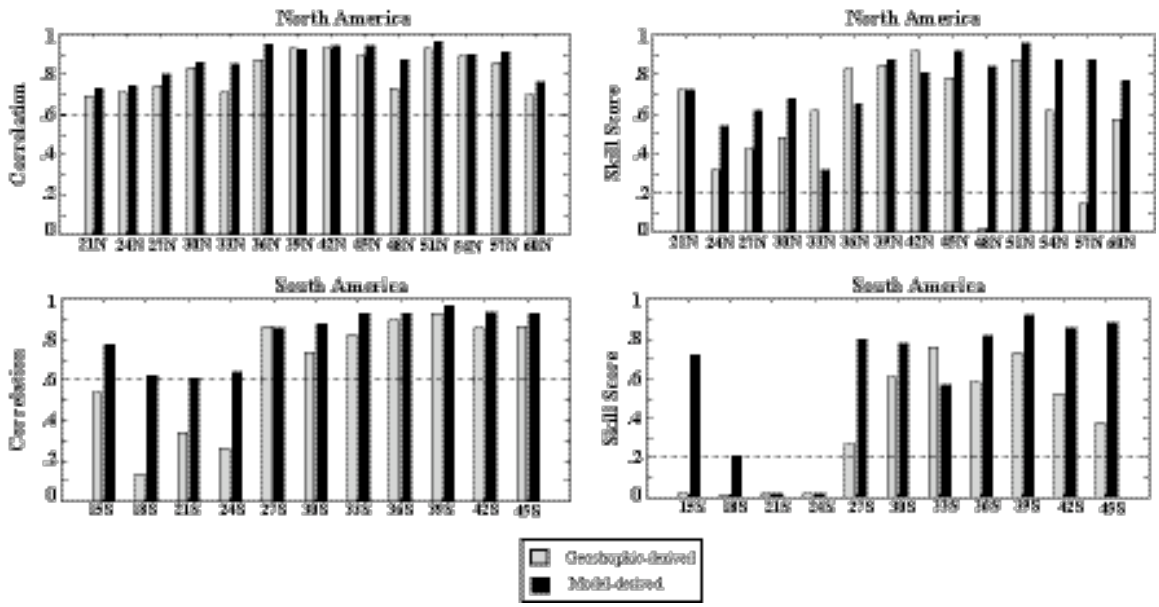

Figure 14. Correlation coefficients and skill scores for geostrophic-derived (gray bars) and model-derived (black bars) upwelling estimates. Upper left panel shows correlation between derived estimates and satellite estimates at the North American sites. Lower left panel shows correlations for the South American sites. Upper right panel shows skill scores for the derived estimates at the North American sites. Lower right shows skill scores for the South American sites. Dashed lines represent significance levels based on Murphy and Epstein, 1989.

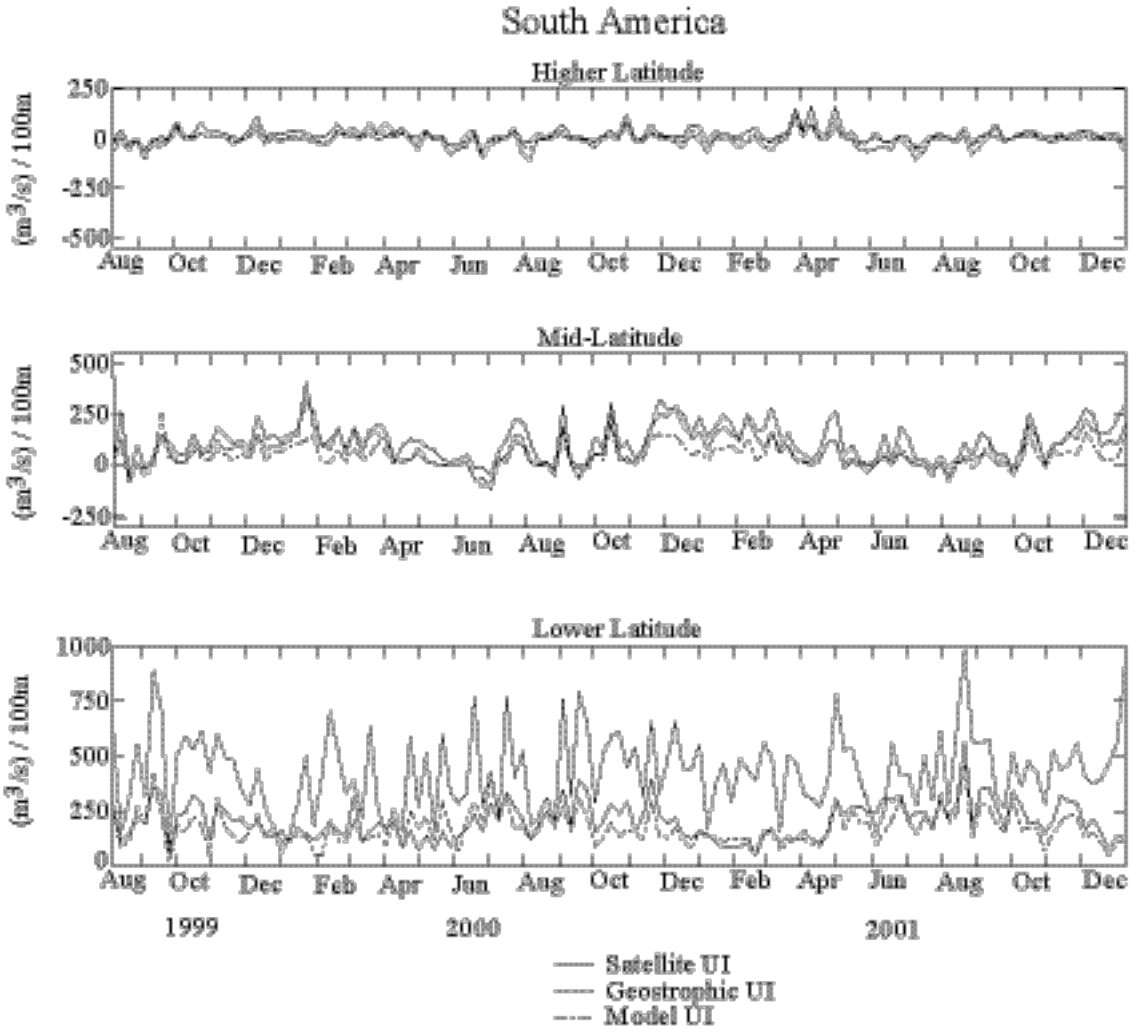

Figure 15. Upwelling estimates at three South American sites based on satellite-measured (solid line), geostrophic-derived (dashed line), and model-derived (dash-dot line) surface winds. The higher latitude site is 42°S, 76°W (off southern Chile), the mid-latitude site is 33°S, 73°W (near Valparaiso, Chile), and the lower latitude site is 15°S, 77°W (near Lima, Peru).

Table 4. Characteristics of geostrophic-derived upwelling estimates off the west coasts of North and South America.

North America (Lat, Lon)	**Record Length** (weeks)	**Mean upwelling from measured winds (+/-Std.Dev.)** (m^3/s) per 100m	**Mean upwelling from geostrophic winds (+/ Std.Dev.)** (m^3/s) per 100m	**Bias** (m^3/s) per 100m	**Correlation**	**Skill Score**
60N,146W	127	-23 (+/- 36)	-33 (+/- 41)	-10	**0.70**	**0.57**
57N,137W	127	-22 (+/- 37)	-51 (+/- 63)	-29	**0.86**	0.15
54N,134W	127	-24 (+/- 43)	-42 (+/- 64)	-18	**0.89**	**0.62**
51N,131W	127	-6 (+/- 47)	-19 (+/- 56)	-13	**0.93**	**0.87**
48N,125W	127	0 (+/- 20)	-17 (+/- 44)	-17	**0.73**	< 0
45N,125W	127	11 (+/- 46)	-9 (+/- 56)	-20	**0.89**	**0.78**
42N,125W	127	58 (+/- 105)	47 (+/- 113)	-11	**0.93**	**0.92**
39N,125W	127	105 (+/- 111)	88 (+/- 139)	-17	**0.93**	**0.85**
36N,122W	127	87 (+/- 75)	66 (+/- 73)	-21	**0.87**	**0.83**
33N,119W	126	67 (+/- 40)	55 (+/- 49)	-12	**0.71**	**0.62**
30N,119W	126	85 (+/- 42)	49 (+/- 34)	-36	**0.83**	**0.48**
27N,116W	127	106 (+/- 45)	69 (+/- 38)	-37	**0.74**	**0.42**
24N,113W	127	92 (+/- 35)	68 (+/- 47)	-24	**0.71**	**0.32**
21N,107W	127	50 (+/- 52)	42 (+/- 42)	-8	**0.69**	**0.72**
South America						
15S, 77W	127	204 (+/- 85)	432 (+/- 182)	228	0.54	< 0
18S, 73W	127	89 (+/- 30)	172 (+/- 93)	83	0.13	< 0
21S, 72W	127	85 (+/- 28)	5 (+/- 15)	-80	0.34	< 0
24S, 72W	127	109 (+/- 46)	65 (+/- 49)	-44	0.26	< 0
27S, 73W	127	113 (+/- 59)	52 (+/- 44)	-61	**0.87**	**0.27**
30S, 73W	127	125 (+/- 77)	127 (+/- 101)	2	**0.74**	**0.61**
33S, 73W	127	105 (+/- 86)	77 (+/- 94)	-28	**0.83**	**0.76**
36S, 74W	127	85 (+/- 86)	23 (+/- 97)	-62	**0.90**	**0.58**
39S, 75W	127	37 (+/- 66)	-5 (+/- 72)	-42	**0.93**	**0.73**
42S, 76W	127	19 (+/- 36)	-11 (+/- 35)	-30	**0.86**	**0.52**
45S, 76W	127	5 (+/- 35)	-29 (+/- 40)	-34	**0.87**	**0.38**

* Bold values have predictive value (correlation greater than 0.6 or skill score greater than 0.2; Murphy and Epstein, 1989).

Table 5. Characteristics of model-derived upwelling estimates off the west coasts of North and South America.

North America (Lat, Lon)	**Record Length** (weeks)	**Mean upwelling from measured winds (+/- Std.Dev.)** (m^3/s) per 100m	**Mean upwelling from model winds (+/- Std.Dev.)** (m^3/s) per 100m	**Bias** (m^3/s) per 100m	**Correlation** (0-1)	**Skill Score** (0-1)
60N,146W	127	-20 (+/- 40)	-25 (+/- 33)	-5	**0.76**	**0.77**
57N,137W	127	-21 (+/- 38)	-29 (+/- 40)	-8	**0.91**	**0.87**
54N,134W	127	-24 (+/- 43)	-16 (+/- 31)	8	**0.90**	**0.87**
51N,131W	127	-5 (+/- 46)	0 (+/- 38)	5	**0.96**	**0.96**
48N,125W	127	0 (+/- 21)	-4 (+/- 15)	-4	**0.87**	**0.84**
45N,125W	127	10 (+/- 47)	-1 (+/- 39)	-11	**0.94**	**0.92**
42N,125W	127	57 (+/- 107)	14 (+/- 64)	-43	**0.94**	**0.81**
39N,125W	127	106 (+/- 111)	71 (+/- 94)	-35	**0.92**	**0.87**
36N,122W	127	86 (+/- 75)	36 (+/- 39)	-50	**0.95**	**0.65**
33N,119W	126	67 (+/- 41)	24 (+/- 24)	-43	**0.85**	**0.32**
30N,119W	126	84 (+/- 43)	57 (+/- 34)	-27	**0.86**	**0.68**
27N,116W	127	106 (+/- 44)	78 (+/- 37)	-28	**0.80**	**0.62**
24N,113W	127	92 (+/- 36)	70 (+/- 37)	-22	**0.74**	**0.54**
21N,107W	127	51 (+/- 52)	33 (+/- 35)	-18	**0.73**	**0.72**
South America						
15S, 77W	127	204 (+/- 85)	174 (+/- 77)	-30	**0.78**	**0.72**
18S, 73W	127	90 (+/- 29)	66 (+/- 33)	-24	**0.62**	**0.21**
21S, 72W	127	85 (+/- 28)	45 (+/- 28)	-40	**0.61**	< 0
24S, 72W	127	110 (+/- 46)	55 (+/- 42)	-55	**0.64**	< 0
27S, 73W	127	113 (+/- 58)	98 (+/- 61)	-15	**0.86**	**0.80**
30S, 73W	127	126 (+/- 79)	85 (+/- 72)	-41	**0.88**	**0.78**
33S, 73W	127	106 (+/- 86)	39 (+/- 62)	-67	**0.93**	**0.57**
36S, 74W	127	84 (+/- 84)	47 (+/- 79)	-37	**0.93**	**0.82**
39S, 75W	127	37 (+/- 65)	16 (+/- 62)	-21	**0.97**	**0.92**
42S, 76W	127	19 (+/- 36)	6 (+/- 30)	-13	**0.94**	**0.86**
45S, 76W	127	5 (+/- 35)	-7 (+/- 30)	-12	**0.93**	**0.88**

***** Bold values have predictive value (correlation greater than 0.6 or skill score greater than 0.2; Murphy and Epstein, 1989).

THIS PAGE INTENTIONALLY LEFT BLANK

IV. EKMAN TRANSPORT AND PUMPING IN THE CALIFORNIA CURRENT BASED ON THE U.S. NAVY'S HIGH-RESOLUTION ATMOSPHERIC MODEL (COAMPS)[2]

A. INTRODUCTION

The motive for this study was to evaluate the NOAA Pacific Fisheries Environmental Laboratory's routine upwelling estimates [Bakun, 1973; Schwing et al., 1996; Norton et al., 2001, Norton et al., 2002]. These estimates within eastern boundary currents are important because upwelling increases biological productivity. As a result of this productivity, fisheries in coastal upwelling regions provide more than one-third of the world's total marine fish catch [Food and Agriculture Organization of the United Nations, 1995]. Historically these upwelling estimates used pressure analyses from large-scale (~300 km) atmospheric models to estimate geostrophic winds [Bakun, 1973; Schwing et al., 1996]. Although NOAA's current operational upwelling estimates (available at http://www.pfeg.noaa.gov/products/las.html) are based on higher resolution pressure fields (~100 km), effects of smaller-scale, non-geostrophic wind patterns, such as those around coastal promontories [Dorman et al., 2000], are missed. These smaller-scale features can either add to, or subtract from, larger-scale upwelling estimated from operational atmospheric models. Our results suggest that these neglected small-scale wind events are just as important as the large-scale features in generating coastal upwelling.

Wind-driven upwelling can be separated into two processes [Sverdrup et al., 1942; Yoshida, 1955; Smith, 1968]. In the first process, called Ekman transport, uniform alongshore winds push surface water either on or offshore due to the earth's rotation. This effect can force surface coastal water downward, or bring nutrient-rich deeper water upward. Present NOAA upwelling estimates are based solely upon this process [Bakun, 1973], and neglect the second process called Ekman pumping. In Ekman pumping, wind-stress curl generates ocean-surface divergence, or convergence, which forces water upward or downward. In the open ocean this results in large-scale upwelling in the center of low-pressure areas, and downwelling in high-pressure areas.

[2] Published in Journal of Geophysical Research, Vol. 108, No. C10, 3327, doi:10.1029/2003JC001902, 2003.

Both of the above processes have been well documented within the California Current system. Halpern [1976a, 1976b] examined winds and hydrographic data from moorings and shipboard observations off central Oregon. He found Ekman transport less important than Ekman pumping in the region, and estimated vertical velocities around 1 m d^{-1} for Ekman transport and 9 m d^{-1} for Ekman pumping. Nelson [1977] examined wind-stress curl in the California Current by compiling historical shipboard wind observations into monthly mean, one-degree squares. His compilation showed positive wind-stress curl near shore, negative curl offshore, and a zero-curl line parallel to the coast some 200 to 300 km offshore. Chelton [1982] related wind-stress curl between San Francisco and northern Baja California to seasonal distributions of zooplankton. Based on this relationship, he suggested Ekman pumping was important for controlling these populations by bringing nutrients up into surface waters. Rudnick and Davis [1988] used moored current meters near Point Arena, California to deduce vertical velocities from horizontal current measurements. They estimated that total springtime upwelling from the combination of both Ekman transport and pumping could be as high as 17 m d^{-1} in this particular area. Bakun and Nelson [1991] sorted Nelson's [1977] original data into higher spatial resolution seasonal averages, and found wind-stress curl maxima near Cape Mendocino, California and in the Southern California Bight.

The above studies have documented areas of wind-stress curl and upwelling near coastal promontories and headlands in the California Current region. These locations, with their rugged topography, tend to deflect alongshore surface winds, and force them to converge and accelerate as they flow by offshore. Dorman et al. [1995] used aircraft observations off Point Arena, California to confirm this effect, and to conclude that it enhanced wind-stress curl and Ekman pumping. Enriquez and Friehe [1995] used aircraft-measured winds to locate a positive wind-stress curl region just west of Point Arena. They then applied a numerical model to the data and demonstrated that the observed wind-stress curl would significantly enhance local upwelling. Burk and Thompson [1996] and Cui et al. [1998] used numerical wind models to map locally enhanced wind regions off central California. In the Southern California Bight, Winant and Dorman [1997], using ship and buoy observations, found that wind data on the scale

of ten kilometers are required to accurately map near-shore conditions. Tjernstrom and Grisogono [2000], using a 3-km-resolution model in conjunction with detailed aircraft data, showed that wind-stress curl south of Cape Mendocino resulted in sea-surface temperature reductions of more than 5°C. Koracin and Dorman [2001] found that wind-stress curl could even be inferred from satellite cloud images near major capes from Oregon to California. And finally, in a recent study similar to ours, Samelson et al. [2002] used a 12-km-grid wind model and satellite data off the Oregon coast to uncover enhanced regions of alongshore wind and wind-stress curl near Cape Blanco. Their conclusion was that these small regions would intensify, and perhaps even control, local upwelling.

All the above studies confirm that coastal promontories induce localized wind effects, which in turn lead to corresponding regions of increased Ekman transport and pumping. Also clear from these studies is that the scale of such areas is too small to be depicted in present-day operational atmospheric models. Moreover, since these areas are not in the operational models, their contributions are not included in NOAA's upwelling estimates. Hence, examining the effect of excluding these intense, sub-grid, wind regions was one of the prime objectives of our study. To do this, we analyzed fine-scale surface winds within the California Current system for a year and a half using a verified 9-km-grid atmospheric model. Our results show that wind-stress curl generates large local vertical velocities and provides at least half the upwelling transport within the California Current system.

B. DATA

1. Model Output

To provide winds for our analysis, we used the US Navy's high-resolution atmospheric model (Coupled Ocean/Atmospheric Mesoscale Prediction System or COAMPS) [Hodur, 1997]. By using progressively finer nested grids of 81, 27 and 9 km, this regional model was capable of resolving the small-scale wind patterns induced by irregular coastlines or coastal topography. We used the 9-km grid because Winant and Dorman [1997] had previously found wind features in the region that required at least 10-km data to resolve. Model forecasts were hourly over the 81 and 27-km grids, with new winds from buoys, ships, and coastal stations assimilated every 12 hours. The 9-km-grid

output is currently available in hind-cast mode only, so for this study we used the model reanalysis done by Kindle et al. [2002].

Several studies have verified this model, and used it to investigate wind patterns along sections of the California coast [e.g. Burk et al., 1999; Dorman et al., 1999; Haack et al., 2001]. Dorman et al. [2000] compared the model output to two months of aircraft wind observations off northern California. They found model and aircraft-derived wind patterns were similar, with both showing maximum winds in the lee of all major capes. Kindle et al. [2002] compared 5-day model wind averages to buoy winds, and found the model accurately reproduced a roll-off in near-shore winds close to Monterey Bay. Chao et al. [2003] also compared the model's winds with buoy observations near Monterey Bay and found the model's daily averaged wind components matched the buoy's within 2.0 m s^{-1} rms.

Since the above tests had confirmed this particular model's capability to depict small-scale wind patterns, we decided to use it to analyze near-shore surface winds within the California Current system. Our test area was between 32°N and 44°N, and offshore to 130°W (region in Figure 16). The model was run continuously from 1 May 1999 to 30 September 2000, and provided a 9-km grid of winds at 10 m above the ocean surface every six hours. The 17-month interval over which the model was run was the longest period available at the time. From the six-hourly model output, we calculated weekly averaged wind components using the 00, 06, 12, and 18 UTC winds for every grid point in the test area. We decided to use weekly averages in order to obtain good estimates of wind-stress curl at time scales required for upwelling development [Allen, 1973].

2. Model Validation

Before using the model winds, we first verified them by comparing weekly averaged components to those from satellite observations at 13 locations (squares and circles in Figure 16). Nine of the verification locations (squares) were at NOAA buoy sites. These sites were mostly near-shore, and ranged from 8 to 41 km from the coast and from 100 to 200 km apart north to south. Since the winds recorded by these buoys are not only accurate (1 m s^{-1}, 10 degrees) [Hamilton, 1980] but also routinely assimilated into the model, we expected good agreement at these locations. The other four verification locations (circles in Figure 16) were further offshore. They were at sites where NOAA

provides routine upwelling estimates, and ranged from 35 to 110 km from the coast and were separated by about 300 km north-south. NOAA's upwelling estimates at these four sites, also called upwelling indices, use geostrophic winds estimated from the pressure-field analysis of a global US Navy model [Bakun, 1973]. A friction correction (30% speed reduction, 15 degree shift) is applied to these geostrophic winds before the upwelling estimate is calculated.

The satellite wind data used for model verification were from the polar-orbiting QuikSCAT satellite. The particular set of data we used is referred to by NASA as Level 2B swath data [Jet Propulsion Laboratory, 2001]. Tests have shown it to be the most accurate of the several data sets available. In comparisons with buoy-measured winds in the same area off the US west coast, this data set agreed with buoy-measured winds within 1.3 m s^{-1} and 26 degrees rms [Pickett et. al, 2003]. During operation, wind speed and direction are estimated from the properties of a radar scatterometer signal that the satellite bounces off the ocean surface. The signal irradiates a roughly 25 km ocean area and thus provides average wind speed over this area. The transmitting antenna rotates in order to view the ocean surface from a variety of angles to estimate wind direction. Owing to the satellite's speed and orbit, wind observations are repeated for every 25 km ocean area once every 12 hours. Because of the radar's technology, the satellite cannot provide accurate wind measurements within 25 km of shore (land in viewing area), in rain (scattered return signal), or at low wind speeds (poor directionality). Although these satellite wind data have been available from NASA's web site (http://podaac.jpl.nasa.gov/quikscat) since August 1999, they are not yet assimilated into Navy models.

At each of the 13 validation sites, satellite observations were selected so that the validation site was within the 25 km viewing area. If this area contained land, the closest adjacent viewing area without land was selected. The effect on accuracy of this small shift in position has been shown to be minor [Pickett et al., 2003]. Next, the selected observations were edited by discarding data when the satellite detected rain, and when wind speeds were less than 3 m s^{-1}. Also, a nine-degree clockwise direction bias in the satellite data, measured in tests in the same region [Pickett et al., 2003], was removed.

Finally, the remaining 12-hourly satellite wind components were weekly averaged to match the similarly averaged model winds. This was done for each of the 13 validation sites from August 1999 to September 2000.

After the above editing and matching, we had about 60 pairs of model and satellite-derived weekly averaged wind components at each of the 13 validation sites. For the entire test period, we had 789 comparisons. Table 6 lists satellite-model differences and correlation coefficients at each of the sites. The satellite-model differences at the nine buoy locations were 1.7 m s^{-1} rms for the eastward component and 1.8 m s^{-1} rms for the northward component. The differences at the four NOAA upwelling sites were 1.6 m s^{-1} rms eastward and 1.2 m s^{-1} rms northward. The model appeared to perform equally well at the nine sites where buoy data were assimilated as it did at the four independent sites. The differences for the 13 validation sites combined were 1.7 m s^{-1} rms eastward, and 1.6 m s^{-1} rms northward. Also, model and satellite wind components were significantly correlated (95% level) at all 13 sites.

In addition to the point-to-point comparisons at the above validation sites, we also tested the model's ability to accurately depict wind gradients. This was necessary since gradients were critical in our wind-stress curl calculations. The gradient check was done by computing the difference in the weekly northward wind components between a buoy 15 km off Point Arena, and satellite observations 115 km offshore (the circle and square in Figure 16 slightly north of Point Arena). This location was used because it was the only place in the study area that had a large near-shore wind gradient as well as a buoy located very close to shore. Buoy data were necessary near shore because the QuikSCAT satellite cannot measure winds within 25 km of shore. The measured wind gradient at these two sites was then compared to the model gradient from grid points closest to the observed sites. The observed and model gradients were then compared for each of the 61 weeks (Figure 17). Although the model slightly underestimated the overall mean gradient (0.9 m s^{-1} per 100 km rms), the correlation coefficient between observed and model gradients was 0.9. The overall mean difference between model and observed gradients was 1.6 m s^{-1} per 100 km rms. The total range of gradients for the 61 weeks was -2 to +9

m s^{-1} per 100 km. These results suggested that the model does a reasonable job of estimating near-shore gradients (within roughly 20%), and a good job of tracking these gradients (correlation of 0.9).

3. Upwelling Estimates

After we were convinced that the model was providing reasonable wind speeds, directions, and gradients in our test region, the next step was to estimate upwelling from the model winds. To do this, we first converted the model six-hourly wind components to wind stress using the same bulk formula ($\tau = \rho_a C_d |\boldsymbol{v}| \boldsymbol{v}$) [Gill, 1982], constant air density (1.2 kg m^{-3}), and constant drag coefficient (.0013) that NOAA uses in their estimates. We calculated the eastward and northward stress components at each model grid point within the region for each week of the 74-week test period. These stresses were then used to derive both offshore Ekman transport and Ekman pumping.

The Ekman transport, **M**, was calculated from [Smith, 1968; Bakun, 1973]:

$$\mathbf{M} = \frac{1}{\rho_w f} \boldsymbol{\tau} \times \mathbf{k} \qquad \text{(units = } m^3\ s^{-1} \text{ per meter of coast)}$$

where $\boldsymbol{\tau}$ is the six-hourly wind-stress vector at the grid point nearest to the coast; ρ_w the density of sea water (assumed constant at 1024 kg m^{-3}); f the Coriolis parameter; and **k** the unit vertical vector. The offshore component of the Ekman transport was calculated from the dot product of the above transport vector with an orthogonal to the local coastline. An orthogonal for each coastal grid point was generated by fitting a straight line through a 50 km section of coastline (25 km north and south of coastal point), and then calculating the orthogonal with respect to this line. We ended up with a value of Ekman transport for every coastal grid point.

The Ekman pumping velocity, w, was calculated from [Smith, 1968]:

$$w = \frac{1}{\rho_w f} \nabla \times \boldsymbol{\tau} \qquad \text{(units = m } s^{-1}\text{)}$$

where $\nabla \times \boldsymbol{\tau}$ is the curl of the derived six-hourly wind-stress vector; ρ_w is the density of seawater, and f is the Coriolis parameter. The curl was calculated using centered

derivatives spanning two 9-km grid points, and was set to zero if a grid point was on land. Our tests showed this simple derivative method produced results equivalent to more sophisticated methods.

In order to directly compare the two upwelling processes, we had to first convert Ekman pumping to vertical transport by integrating vertical velocity out to some offshore distance. We chose a 300 km distance based on Nelson's [1977] observation that positive wind-stress curl extended out to this distance in the region.

After the Ekman pumping was converted to vertical transport, we had two independent upwelling estimates: that due to Ekman transport, and that due to integrated Ekman pumping. An Ekman transport estimate was available at every coastal grid point; an integrated Ekman pumping estimate was available for each 300 km orthogonal to every coastal grid point. We then compared these two upwelling estimates at four 300-km-long transects across the California Current. The four transects (lines in Figures 18 and 19) were chosen to intersect NOAA's upwelling sites.

In addition to comparing transports at just the four transects, we also estimated total upwelling and vertical velocities for the entire California Current system. Total upwelling was done by summing the transport estimates from both Ekman transport and pumping along the entire coastline of the test area. Vertical velocity estimates were more indirect and required assumptions. First, we converted Ekman transport to vertical velocity by dividing it by a Rossby radius, the approximate offshore scale of the transport [Allen, 1973]. We used both a 10 and 20 km Rossby radius based on the range of what others have estimated for the region [Allen, 1973; Huyer, 1983; Rosenfeld et al., 1994]. For the 10 km calculation, we used the model wind from the grid point nearest to the coast; for the 20 km calculation, we used the mean wind from the first and second grid points off the coast. The resulting Ekman transport vertical velocity estimates were then compared to Ekman pumping vertical velocity estimates.

C. RESULTS

1. Ekman Transport

The model surface winds during summer (June-August) in the region were typically from the north-northwest at 6 to 10 m s^{-1}. These winds would produce near-shore wind stresses of approximately 0.1 N m^{-2}, which, in turn, would yield offshore

Ekman transports of 1 m^3 s^{-1} per meter. Just south of Cape Blanco, Cape Mendocino, Point Arena, Point Sur, and Point Conception, however, the model showed concentrated patches of both wind speed and wind shear downwind and 10 to 50 km offshore from these promontories. Within these patches, only several grid points in size, weekly averaged model wind speeds up to 18 m s^{-1}, and gradients up to 4 m s^{-1} per 9 km occurred frequently. The calculated weekly averaged wind stress in these areas was often double the background levels, and exceeded 0.2 N m^{-2} (Figure 16 shows a typical summer week). These high stress areas would produce offshore Ekman transports around 2 m^3 s^{-1} per meter. The maximum summer offshore transport estimate was 3 m^3 s^{-1} per meter, and occurred 20 km offshore and 80 km south of Point Arena during 7-14 May 1999.

In contrast to the relatively steady summer winds, model winter winds (December-February) in the test region were more variable. They were 4 to 8 m s^{-1} from the southwest in the southern part of the test area, backing to south and increasing in speed to 6 to 10 m s^{-1} in the northern part. Weekly averaged wind stress values were around 0.1 N m^{-2} in the north, and would produce onshore Ekman transports (downwelling) of about 1 m^3 s^{-1} per meter. Intensification occurred off Cape Blanco and Cape Mendocino, with weekly averaged model wind speeds up to 13 m s^{-1}, and wind-speed gradients up to 2 m s^{-1} per 9 km. Wind stresses reached 0.2 N m^{-2} at these two areas. The maximum winter onshore transport at these two areas was 2 m^3 s^{-1} per meter, and occurred during the week of 7-14 November 1999.

2. Ekman Pumping

During summer, the model typically showed positive (counterclockwise) weekly averaged wind-stress curl on the order of +1 x10^{-6} N m^{-3} along the entire coast, and extending in irregular patches out as far as 300 km (green areas in Figure 18). Adjacent to the high curl areas however, the positive wind-stress curl patches were confined closer to shore. Just south of every major promontory, small concentrated areas of intense positive wind-stress curl hugged the coast. These areas (red, orange, and yellow in Figure 18) frequently had an order of magnitude higher curl (up to +10 x10^{-6} N m^{-3}) than anywhere else in the test area. These high intensity areas appeared every few weeks, and represented small concentrated areas of Ekman pumping with vertical velocities (upwelling) reaching +10 to +15 m d^{-1} in summer.

During winter, weekly averaged wind-stress curl was negative (clockwise) near shore. Thin bands of strongly negative (-2 $x10^{-6}$ N m^{-3}) wind-stress curl were confined to within a few grid points of the coast. Concentrated negative wind-stress curl occurred in bands from Cape Blanco north, and from Point Arena to Cape Mendocino (blue and violet areas in Figure 19). These strong negative bands appeared once every few weeks, frequently reaching -5 $x10^{-6}$ N m^{-3}. The negative wind-stress curl at these two areas was weaker than the similar areas of positive wind-stress curl in summer, but still implied Ekman pumping vertical velocities (downwelling) of -4 to -6 m d^{-1}.

The seasonal contrast can be seen clearly in Figure 20. In this figure vertical velocity is plotted against distance offshore at the four transects (red lines in Figures 18 and 19) for a typical summer and winter week (14-21 July 2000 and 14-21 January 2000). These plots show three things: First, the strongest upwelling is always confined within 50 km of shore. Second, there are major seasonal differences, with upwelling common in the summer and downwelling in winter. Third, there is considerable variation depending on location within the test area. The two northern transects are similar, but the middle transect, located just south of Point Sur, shows the strong summer upwelling, downwelling offshore from this upwelling, and nothing in the winter. The southernmost transect, where winds were weakest, shows only very little diffuse upwelling.

3. Transport and Pumping Comparisons

Weekly variations in vertical transport, integrated over the whole length of each of the four transects, are shown in Figure 21. Ekman pumping was generally larger and more variable than Ekman transport. At the three northern transects there was a seasonal variation, with higher positive transport in summer and periods of negative transport in winter. At the southernmost transect, in the Southern California Bight, the vertical transport was always positive and almost all due to Ekman pumping.

To compare our model-derived upwelling to the values published by NOAA, we added both transports, and matched the results to NOAA's upwelling values (Figure 22). Generally, NOAA estimates agreed well with model-derived estimates and had similar means and seasonal variations. NOAA estimates were significantly correlated (95% level) with model-derived transport at all four transects. The highest correlation was 0.9 at the northern transect, and the lowest was 0.6 at the southern transect. At the two

northern transects, however, the NOAA estimates often deviated considerably from those of the model by overestimating highs and lows.

In spite of the fact that NOAA upwelling estimates exclude Ekman pumping, they were closer to the model-derived total transport than one might expect. One explanation may be that NOAA bases its geostrophic wind on grid points 100 km offshore. Since wind speeds generally increase with offshore distance, NOAA's wind estimate for the coastal region will be too high. High winds, in turn, lead to overestimates of Ekman transport, which may compensate for the excluded Ekman pumping.

4. System-wide Upwelling

By adding up the Ekman transport for all the shoreline grid points and Ekman pumping for all the 300 km orthogonals at each grid point, we could compare the relative power of the two processes within the test area. Figure 23 shows the month-to-month variations in Ekman transport, Ekman pumping transport, and their sum. Ekman pumping is the dominant process, generally about double the Ekman transport. Only during the system-wide downwelling events (November 1999, January 2000, February 2000) are the two processes similar. The same transport data shown in Figure 24 are compiled by seasons in Figure 24 and itemized in Table 7. During summer (June-August) Ekman transport, Ekman pumping, and total transport are at their maximum. During winter (December-February) the opposite is true, with all transport values at their minimum and Ekman transport even being negative. Ekman pumping still remains positive in winter, but is small. Total transport ranged from $2x10^6$ m^3 s^{-1} in summer to near zero in winter.

5. Upwelling Velocities

By assuming that the major Ekman transport occurred within either the first 10 or 20 km of shore, we could make an estimate of the vertical velocity implied by this transport. This allowed us to compare the vertical velocities of two Ekman processes. We found from these estimations that both processes produce vertical velocities on the same order of magnitude. Figure 25 compares vertical velocity estimates from both processes during summer at the Point Sur transect. In the near-shore upwelling zone both mechanisms had similar peak vertical velocities (around +10 m d^{-1}), suggesting that net vertical velocity in this particular region depends about equally on both processes. The figure also shows in the top and bottom panels that our velocity estimates were not very

sensitive to the offshore extent of Ekman transport since the increase in wind stress with offshore distance tends to compensate for the larger length scale.

D. DISCUSSION

We found that the output of the US Navy's high-resolution atmospheric model was sufficiently detailed and accurate to reveal the fine-scale structure of near-shore winds and wind-stress curl within the California Current system. Others have also confirmed this ability of the model [e.g. Dorman et al., 1999; Dorman et al., 2000; Hack et al., 2001]. These past studies, as well as our own, show major coastal promontories perturb the large-scale flow, and generate bands of high wind and strong wind-stress curl. These bands are typically less than the grid size of conventional wind models, and are therefore missed or aliased in operational forecasts.

Our study showed five major promontories (Cape Blanco, Cape Mendocino, Point Arena, Point Sur, and Point Conception) are responsible for intensifying the alongshore wind stress and wind-stress curl. This effect of the five locations has also been confirmed by Dorman et al. [1995, 2000] and Enriquez and Friehe [1995]. The local wind intensifications increase both offshore Ekman transport and Ekman pumping. We estimated that near these promontories upwelling velocity induced by wind-stress-curl was comparable to that induced by Ekman transport. This implies that total upwelling within these narrow near-shore bands is much greater than that in surrounding areas. This is supported by Kelly [1985], who noted that satellite-observed cold-water plumes off northern California were anchored to coastal topography.

If these wind intensifications and resulting wind-stress curl are always as robust as we found, then they are capable of modifying alongshore current patterns as Hickey [1979] suggested. The cyclonic vorticity injected by wind-stress curl downwind of these promontories in summer would contribute to a poleward surface current. Such a poleward current, with nutrient-rich upwelling water, would collide with the wind-driven surface current and could account for the odd filaments of phytoplankton observed in the region [Abbott and Barksdale, 1991].

Our results also showed that during our year and a half simulation within the California Current system, overall upwelling from wind-stress curl was as large as that from alongshore wind stress. This suggests that Ekman pumping is as powerful an

upwelling mechanism in the region as Ekman transport. Chelton [1982] first proposed this idea when he observed seasonal zooplankton distributions that were related to Ekman pumping instead of alongshore wind stress. Additionally, Strub et al. [1990] using satellite observations and model winds showed that pigment concentrations in the California Current system were more closely related to Ekman pumping than to Ekman transport.

Even though the above fine-scale processes are missing from NOAA's upwelling calculations, their estimates still seem to provide reasonable approximations. Their estimates apparently succeed by applying strong offshore winds to the entire coastal zone. The result, by default, is a partial correction for the missing Ekman pumping. A more accurate, more detailed, and more useful estimate could be obtained by using a high-resolution model similar to what we used. Increased resolution would not only allow Ekman pumping to be included, but would better depict the small-scale, intense upwelling bands we observed. The value to the fishing industry alone, for example, of more detailed and accurate upwelling estimates would be great.

In summary, our model study of the California Current has underscored the importance of coastal promontories in determining properties of the overall system. By concentrating alongshore winds, wind stress, wind-stress curl, and upwelling into small, intense bands, these coastal features apparently influence the currents and biological productivity of the entire region. To validate these conclusions, more high-resolution wind observations need to be collected near these coastal promontories. Also, new upwelling indices should be derived to better represent the fine-scale structure of upwelling in the California Current system.

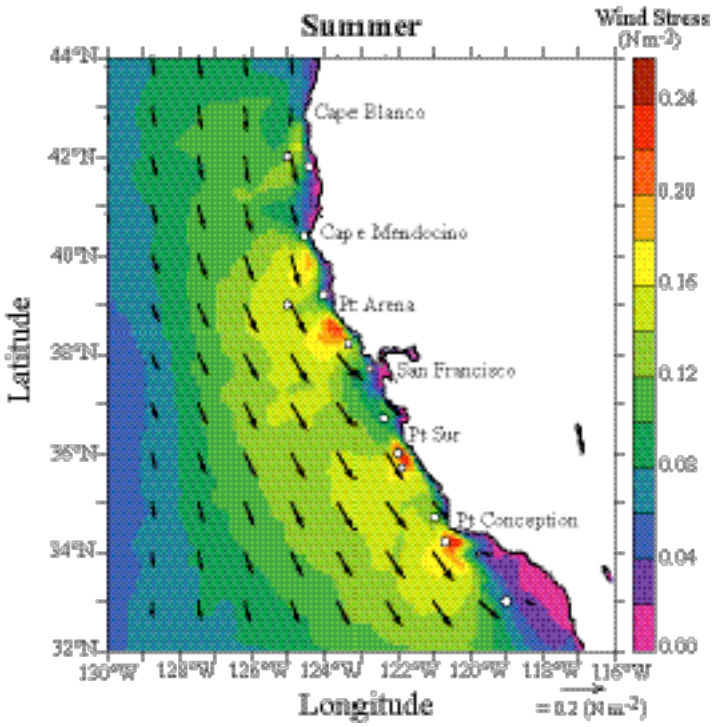

Figure 16. Model-derived weekly averaged wind stress for the period 14-21 July 2000 in the California Current region. The wind stress was derived from the 9 km-grid COAMPS model. Color bands show intensity of averaged wind stress; black vectors show wind stress directions (every 12th vector shown). The model was compared to satellite-measured winds at NOAA buoy sites (squares) and NOAA upwelling sites (circles). Areas of highest wind stress occur south of Cape Mendocino, Point Arena, Point Sur, and Point Conception.

Table 6. COAMPS weekly averaged winds compared with QuikSCAT satellite winds at buoy locations and NOAA upwelling sites.

						RMS Differences	
Validation Site	**Location** (Lat, Lon)	**Distance from shore** (km)	**Number of Observations**	**Correlation** (u-comp.)	**Correlation** (v-comp.)	**u-comp.** (m s-1)	**v-comp.** (m s-1)
Buoy 46027	41.8N, 124.4W	13	58	0.65	0.84	2.4	3.0
Buoy 46030	40.4N, 124.5W	8	60	0.37	0.83	2.8	2.4
Buoy 46014	39.2N, 124.0W	17	61	0.84	0.88	2.2	2.5
Buoy 46013	38.2N, 123.3W	22	61	0.88	0.90	1.5	1.8
Buoy 46026	37.7N, 122.8W	20	61	0.90	0.92	1.1	1.3
Buoy 46042	36.7N, 122.4W	35	61	0.89	0.90	1.2	1.0
Buoy 46028	35.7N, 121.9W	41	61	0.89	0.90	1.4	1.1
Buoy 46023	34.7N, 121.0W	31	61	0.86	0.90	1.2	1.0
Buoy 46063	34.2N, 120.7W	30	61	0.89	0.92	1.2	1.1
Combined			545			1.7 (+/-.2)	1.8 (+/-.2)
Upwelling Site 1	42.0N, 125.0W	55	61	0.70	0.90	1.8	1.5
Upwelling Site 2	39.0N, 125.0W	110	61	0.87	0.90	1.5	1.3
Upwelling Site 3	36.0N, 122.0W	35	61	0.84	0.90	1.5	1.1
Upwelling Site 4	33.0N, 119.0W	110	61	0.82	0.83	1.9	1.3
Combined			244			1.6 (+/-.2)	1.2 (+/-.1)
TOTAL			**789**			**1.7 (+/-.1)**	**1.6 (+/-.1)**

* 95% confidence limits were determined from the standard error.

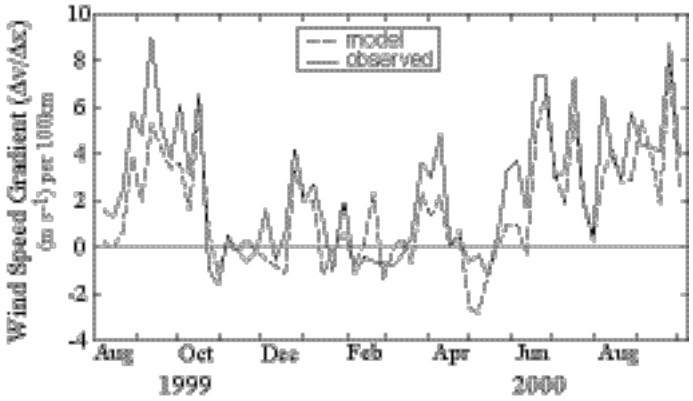

Figure 17. Comparison of observed (solid line) and model (dashed line) wind speed gradients off Point Arena, California. Values are based on the differences between weekly averaged northward wind components at 15 and 115 km offshore. Correlation between the observed and model gradients was 0.9, and the RMS difference was 1.6 m s^{-1}.

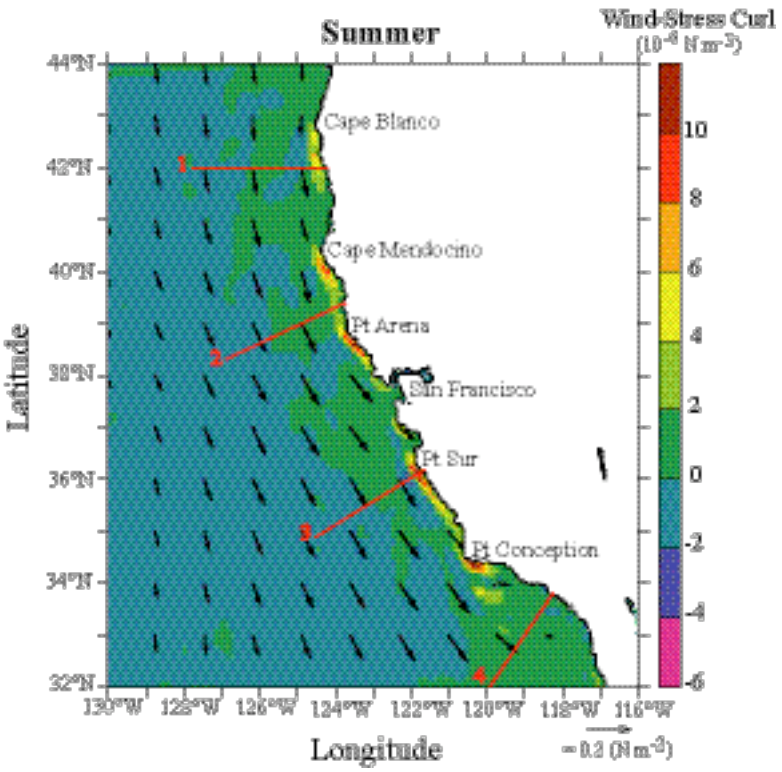

Figure 18. Model-derived weekly averaged wind-stress curl for the period 14-21 July 2000 in the California Current region. The wind-stress curl was derived from the 9 km-grid COAMPS model. Color bands show intensity of averaged wind-stress curl; black vectors show wind stress directions (every 12th vector shown). Areas of highest weekly averaged wind-stress curl occur just south of Cape Mendocino, Point Arena, Point Sur, and Point Conception. Red lines are transects (300 km long) for comparing upwelling transports.

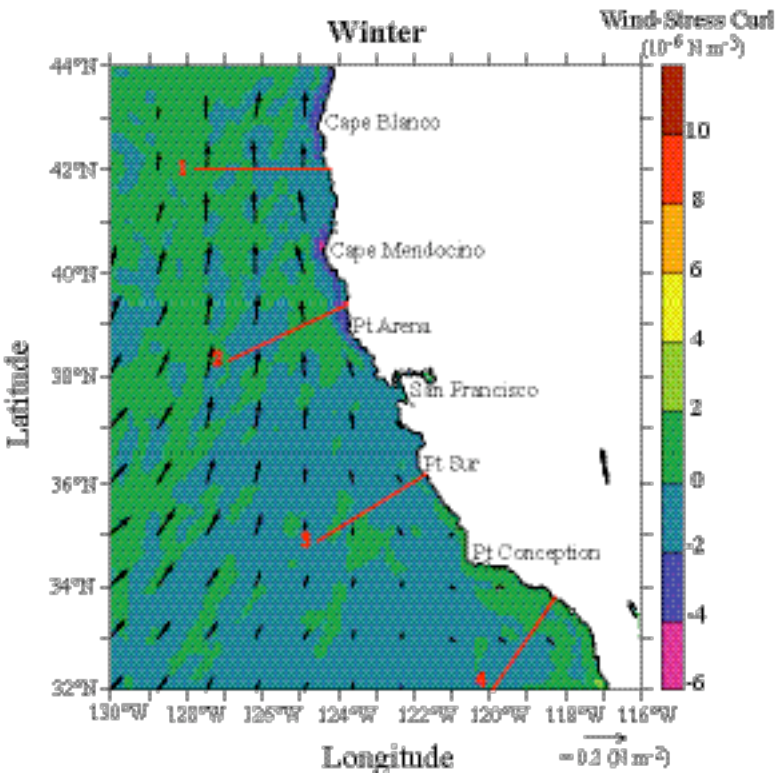

Figure 19. Model-derived weekly averaged wind-stress curl for the period 14-21 January 2000 in the California Current region. The wind-stress curl was derived from the 9 km-grid COAMPS model. Color bands show intensity of averaged wind-stress curl; black vectors show wind stress directions (every 12th vector shown). Areas of negative weekly averaged wind-stress curl occur near Point Arena, Cape Mendocino, and Cape Blanco. Red lines are transects (300 km long) for comparing upwelling transports.

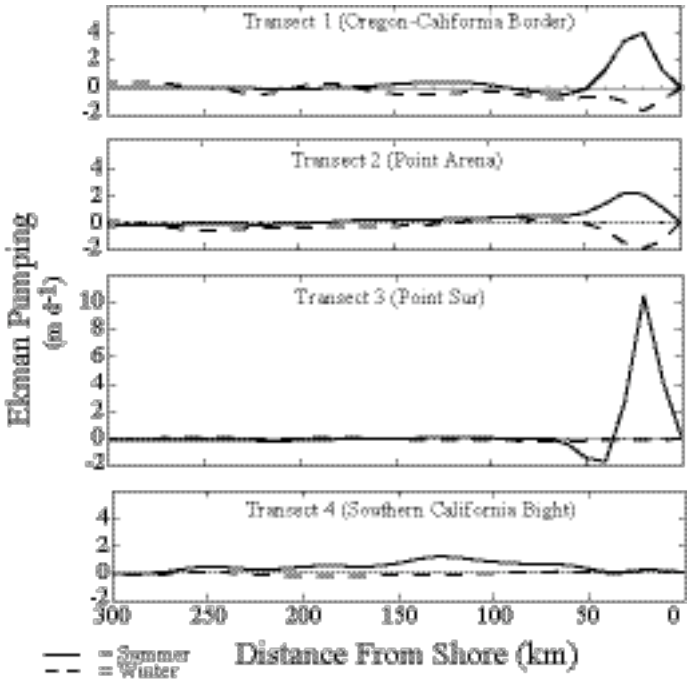

Figure 20. Ekman pumping at four transects through the California Current, based on weekly averaged wind from the 9 km-grid COAMPS model (refer to Figure 19 for locations of transects). The solid line is curl-induced vertical velocity for a typical week in summer (14-21 July 2000); the dashed line is for a typical week in winter (14-21 January 2000).

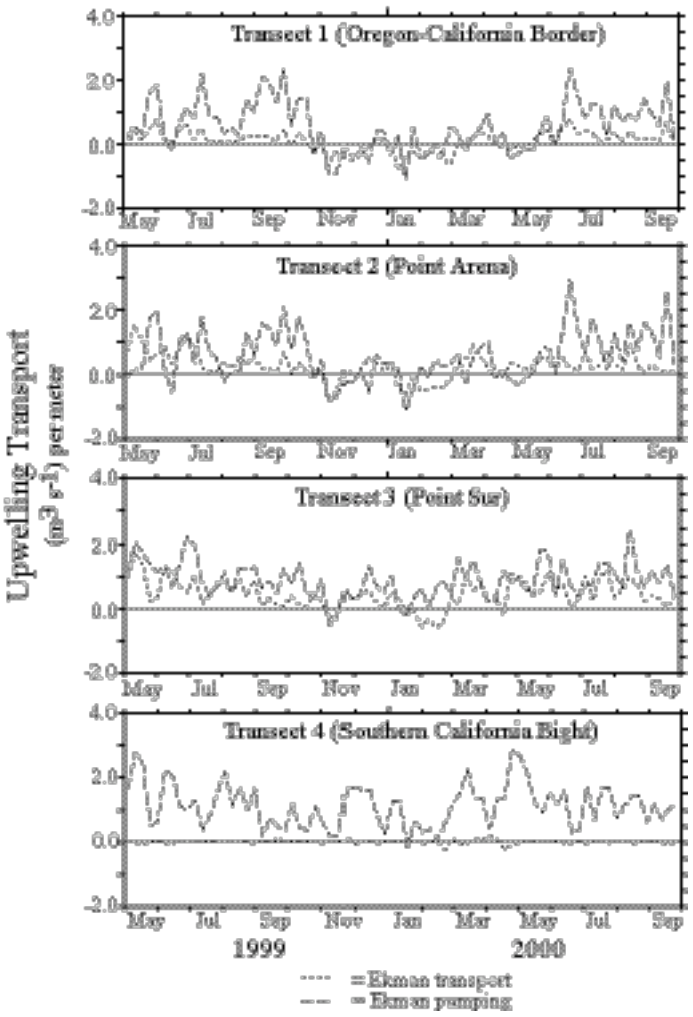

Figure 21. Time series of Ekman transport (dotted line) and integrated Ekman pumping (dashed line) across four transects through the California Current. Integrated Ekman pumping due to wind-stress curl is the major contributor at all four locations. Data were based on weekly averaged winds from the 9-km-grid COAMPS model.

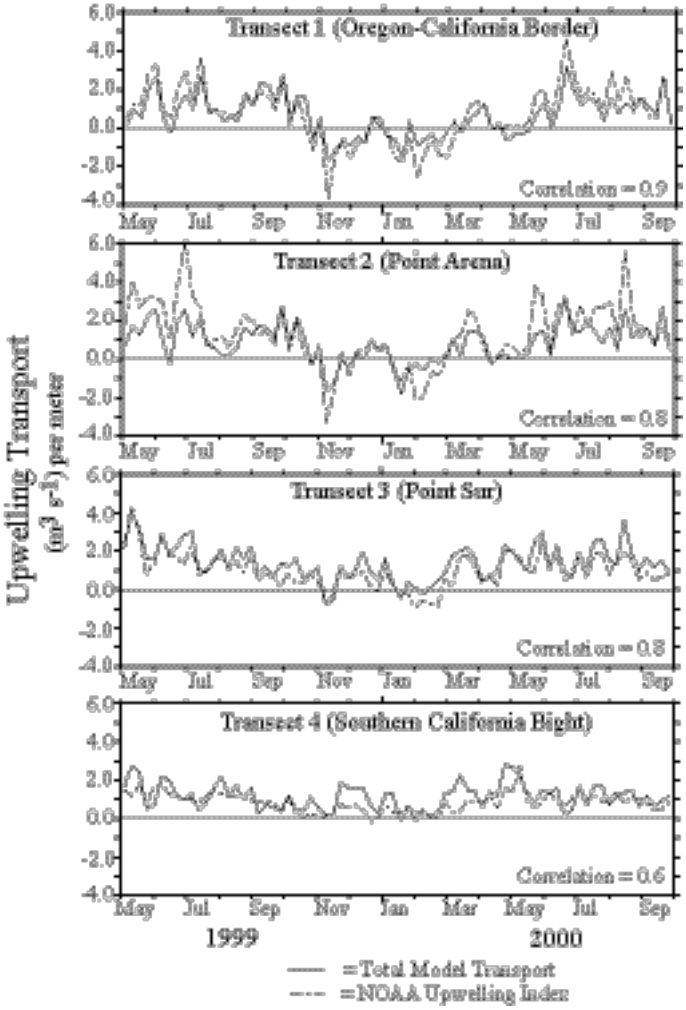

Figure 22. Time series of model-derived, weekly averaged total transport (solid line) and NOAA upwelling index (dash-dot line) across four transects through the California Current.

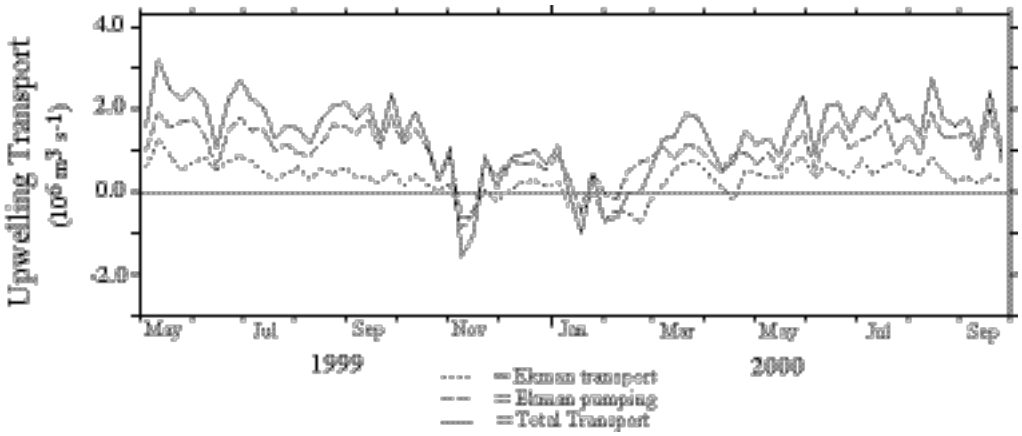

Figure 23. Time series of model-derived, weekly averaged upwelling integrated over the study region. Total Ekman transport is the dotted line; total Ekman pumping is the dashed line; the sum is the solid line. Summer upwelling produces roughly $+2x10^6$ m^3 s^{-1} of transport, whereas winter downwelling produces around $-1x10^6$ m^3 s^{-1}. Seasonal and monthly variations are shown as well.

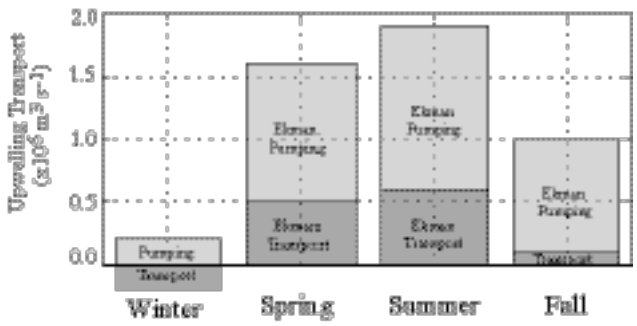

Figure 24. Seasonal upwelling estimates in the California Current. Estimates for Ekman Transport and Ekman Pumping are based on weekly averaged COAMPS high-resolution model winds and are grouped by season as shown in Table 7.

Table 7. Weekly upwelling estimates in the California Current grouped by season. Estimates are based on COAMPS high-resolution model winds.

		Number of Weeks	**Ekman Transport** ($x10^6$ m^3 s^{-1})	**Ekman Pumping** ($x10^6$ m^3 s^{-1})	**Total Transport** ($x10^6$ m^3 s^{-1})
Winter	(Dec-Feb)	13	-.2 (+/-.2)	.4 (+/-.2)	.2 (+/-.4)
Spring	(Mar-May)	17	.5 (+/-.1)	1.1 (+/-.2)	1.6 (+/-.3)
Summer	(Jun-Aug)	27	.6 (+/-.1)	1.3 (+/-.2)	1.9 (+/-.2)
Fall	(Sep-Nov)	17	.1 (+/-.2)	.9 (+/-.4)	1.0 (+/-.5)

* 95% confidence limits were determined from the standard error.

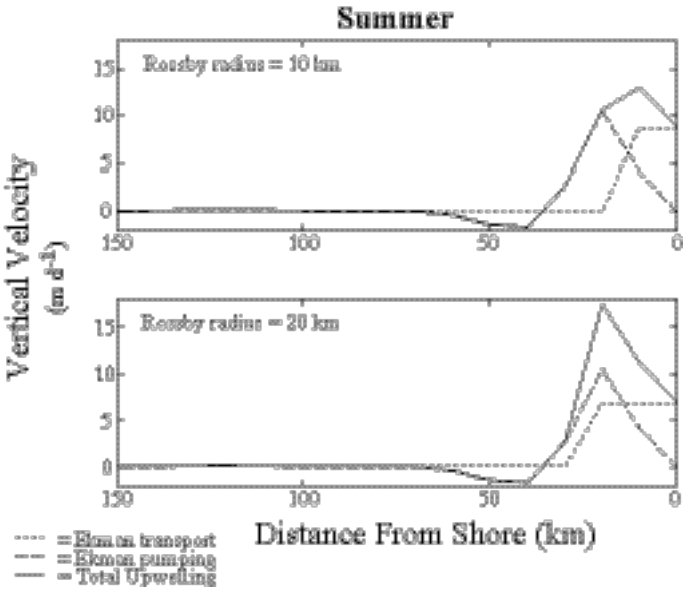

Figure 25. Model-derived, weekly averaged vertical velocity along a transect offshore from Point Sur, California for a typical summer week (14-21 July 2000). Included are the contributions from both Ekman transport and Ekman pumping. Both processes contribute similar vertical velocities. The top figure assumed a 10 km Rossby radius; the bottom a 20 km radius.

THIS PAGE INTENTIONALLY LEFT BLANK

V. SUMMARY AND CONCLUSIONS

A. PROJECT SUMMARY

This dissertation has reviewed the development of present day coastal upwelling estimates, demonstrated how they can be improved, and analyzed the fine scale structure of upwelling overlooked in present day estimates. The study consisted of three phases. In the first phase, the near-shore accuracy of a satellite scatterometer, used as a reference source of wind data, was established by comparing it to buoy-measured winds. In the second phase, the verified satellite-measured winds were used to test a global atmospheric model as a source of surface wind data for use in upwelling estimates. In the third phase, a high-spatial resolution wind model was used to investigate the fine structure of coastal upwelling. Results of each phase are reviewed briefly below.

1. Accuracy of Satellite-Measured Winds

An accurate source of near-shore wind measurements was needed to test proposed improvements in coastal upwelling estimates. The QuikSCAT satellite, in operation since August 1999, offered the advantage of real-time coverage of all the world's coastal zones. However, its near-shore wind accuracy had not been determined. To determine its accuracy, outputs from three different methods of processing the satellite data were compared to buoy-measured winds at 12 near-shore and 3 offshore U.S. west coast buoys. Satellite observations within 25 km and 30 minutes of these buoys were used in the comparisons. Results showed that the scientifically processed swath data produced the most accurate coastal wind data, and that errors in satellite-measured wind were larger near-shore than offshore. All errors, however, could be reduced by discarding winds recorded in rain and in calm to light winds. Rain interfered with the satellite's wind speed estimates derived from surface-roughness, and light winds made it difficult for the satellite's wind direction sensor to measure angular variations in surface roughness.

After selecting both the best processing and editing methods for satellite data, the satellite-minus-buoy wind differences near-shore were 1.3 m s^{-1} and 26 degrees RMS. The differences at offshore buoys, using the same processing and editing technique, were 1.0 m s^{-1} and 15 degrees RMS. In summary, satellite-buoy comparisons showed that by

using the proper processing method and minor editing the QuikSCAT satellite can provide accurate coastal wind data on a global basis.

2. Accuracy of Upwelling Estimates

The second phase of this study explored a method to improve the accuracy of the PFEL upwelling index. These indices, or upwelling estimates, have been routinely produced and distributed for the North and South American west coasts since 1946 and 1981 respectively. Wind data used in these indices are currently based on geostrophic estimates from surface pressures extracted from the U.S. Navy's global atmospheric (NOGAPS) model.

To test potential improvements in the PFEL technique, weekly averaged upwelling indices were calculated using the conventional geostrophic-derived winds for two and a half years at 14 North American and 11 South American coastal sites. Next, using the same sites, times, and technique, two other sets of indices were calculated using model-derived and satellite-measured winds. All three sets of upwelling indices were then compared using correlation coefficients and skill scores. The results showed that upwelling indices based on geostrophic-derived winds agreed with those based on satellite-measured winds at 85% of North American and 65% of South American sites. Upwelling indices based on model-derived winds, on the other hand, agreed at 100% of North American sites and 80% of South American sites. These results indicate that the 60 years of historic upwelling indices for North America are reasonably accurate at most locations and therefore offer users a consistent time series. However, upwelling indices calculated from model-derived winds were shown to be accurate in more regions than indices calculated from geostrophic-derived winds.

Although model-based upwelling indices represented an improvement, they were not accurate in all locations. Off South America where the rugged coast veers sharply eastward near the Peru-Chile border, model-based upwelling estimates did poorly. In these locations the model's 100-km resolution apparently was too crude to depict this abrupt coastline change and the resulting wind perturbations.

3. Small-Scale Upwelling - Ekman Pumping

Phase three of this study investigated the fine-scale structure of coastal winds and upwelling missed by the above large-scale estimates. This was done by using high-

resolution winds from a 9-km-grid regional atmospheric model to analyze wind-stress curl in the California Current region off the US west coast. Prior to using these model results, they were verified with satellite-measured winds at 13 sites. These verification tests showed that the model was capable of measuring weekly averaged wind components within 1.7 m s^{-1}, and wind gradients within 1.6 m s^{-1} per 100 km RMS.

Once the high-resolution model was verified, it was used to produce surface wind fields every six hours from May 1999 to September 2000. Next, the wind components at each grid point were averaged for a week to produce weekly mean surface wind fields. These weekly mean wind fields revealed many strong wind and upwelling features below the grid size of present atmospheric models. For example, bands of wind stress and wind-stress curl were discovered adjacent to every major coastal promontory. Their typical size was around 20 km in the offshore direction and about 50 km in the alongshore direction. Based on the wind-stress curl depicted within these bands, upwelling generated within them would be as strong as that produced by the alongshore wind stress. These high-resolution model tests suggest, therefore, that upwelling indices based on conventional methods provide an incomplete picture of coastal upwelling.

B. CONCLUSIONS

By demonstrating that the QuikSCAT satellite can provide accurate near-shore wind measurements, this research identified a valuable tool for coastal studies (Pickett et al., 2003). Although this satellite has been operating since 1999, its coastal wind measurements were rarely used because their accuracy was unknown. Since this investigation was conducted off the North American west coast with its wide variety of coastal topographies, these satellite accuracy results should apply equally well to most of the world's coastal zones. Now that the accuracy of this satellite's wind data has been verified, the U.S. Navy and NOAA, as well as other operational modeling centers can use its data confidently. As an example, the Navy now plans on assimilating QuikSCAT wind measurements into its global model next year.

Although valuable for assimilation into operational meteorological models or use in research, satellite-measured winds are currently unsuitable for routinely calculating upwelling indices. The migrating orbit of a polar satellite does not provide continuous

coverage at any particular site. For example, off the U.S. west coast the QuikSCAT satellite provides wind measurements every 12 hours for three days, followed by a gap of one to two days. At least two of these satellites would be required for uninterrupted coverage. In addition, these satellites are difficult to maintain. For example, the NSCAT satellite, predecessor to QuikSCAT, stopped working after only nine months. In 2003, the Midori 2 which was the planned replacement for QuikSCAT, failed after ten months. Also, the satellite wind sensors, as well as the data processing, are still evolving. As this study noted, three different processing systems are currently being tested for QuikSCAT data, and post-processing was still necessary to remove wind measurements in rain and light winds. Both hardware and software options are now being explored to reduce such problems in future satellites. As of now, however, continuous near-shore satellite wind measurements are not routine. At present, the best option seems to be for operational centers to assimilate available satellite wind measurements into global and regional meteorological models, and to base coastal upwelling indices on the winds from these models.

The assessment of the PFEL upwelling indices carried out in this study showed that although the use of geostrophic-derived winds provided reasonable values at many sites, model-derived winds were consistently better. Not only did model-derived winds provide better indices at the present upwelling sites, but they could also be extended to areas where geostrophic estimates did not work or could not be used. Examples are South American coastal regions with high coastal mountains and locations very close to the equator. This improvement in the derivation of the index, if implemented, should lead to a better understanding of the relationship between upwelling and fisheries productivity.

The last, and perhaps most important, result of this study is that coastal upwelling is strongly influenced by, and perhaps controlled by, features and processes on a smaller scale than PFEL indices cover. These indices now assume that the dominant coastal upwelling process is offshore Ekman transport driven by a large-scale alongshore wind. This study demonstrated that this is not necessarily the case (Pickett and Paduan, 2003). Wind-stress curl adjacent to capes and points is capable of producing upwelling as large as, or larger than, that due to the mean alongshore wind. Moreover, this study also

revealed that these capes and points modify the large-scale alongshore wind by impeding, deflecting, and accelerating it.

The new picture of coastal upwelling that emerged from this study has two parts. The first part consists of large-scale Ekman transport driven by the mean alongshore wind. The second part consists of strong, compact bands of near-shore upwelling downwind from major coastal promontories driven by small-scale wind stress and wind stress curl. Within these compact bands, upwelling can be forced by both Ekman transport and Ekman pumping. To delineate these bands, however, high-resolution wind data are required. At present, neither satellites nor operational models have the necessary resolution. Even though efforts are underway to increase the resolution of future satellite wind measurements, land contamination will always limit a satellite's view close to shore.

The importance of these overlooked bands of upwelling to fisheries productivity will probably turn out to be great. The wind stress and wind-stress curl within these bands is much more intense than previously expected. Also, a common occurrence offshore of these bands is a region of moderate negative curl, which creates surface convergence. This combination of strong near-shore upwelling with offshore convergence should create frontal zones ideal for the aggregation and feeding of fish and marine mammals.

A final implication of the regions of strong near-shore wind-stress curl is the potential influence that these regions may have on the generation and location of offshore-flowing filaments. These features are observed throughout the California Current system and are associated with major coastal headlands. The alongshore variation in curl-driven upwelling, which is strong at the headland locations, can be expected to create cross-shore currents that may, in part, be responsible for filament initiation.

C. RECOMMENDATIONS FOR FURTHER STUDY

This study has documented the accuracy and usefulness of the QuikSCAT satellite's near-shore wind measurements. It has also pointed out the need for improvements in the satellite's wind measurements in rain and light wind. Better hardware and software might eliminate the need for users to do their own editing. Also,

since the current 25-km resolution of the QuikSCAT data was insufficient to resolve the important small-scale features noted in this study, better spatial resolution in future scatterometers would be desirable.

This study has also suggested that PFEL upwelling indices can be improved and extended to more locations by changing the source of wind data from the present geostrophic estimates to winds extracted from models. Based on results from this study, this change should be implemented using the winds from the U.S. Navy's NOGAPS model. Once the conversion is done, new indices should be hind cast and compared with the geostrophic-based indices to evaluate differences during the 20-year period that both types of data have been available. This evaluation would help determine if the new indices provide continuity with the 60-year time series available with the present indices. Also, the new indices could be tested by repeating previous biological studies to see if better matches are obtained between the new index and fisheries productivity. If higher correlations or skill scores were obtained, then the value of the new method would be confirmed.

This study has also demonstrated the importance of small-scale near-shore wind stress and wind-stress curl. Further efforts are now needed to verify these results and confirm their implications. Future studies need to further validate the Navy's high-resolution wind model, as well as other possible contenders, in different areas and at different times. A study patterned after the recent Autonomous Ocean Sampling Network project, which used ship and aircraft data, would be one way to conduct such a validation. Such tests could also help modelers correct any observed deficiencies in high-resolution coastal models.

And finally, this study also made it clear that upwelling indices must include small space scales so that both Ekman transport and Ekman pumping are included. If an accurate picture of coastal upwelling is to emerge, then atmospheric models with a resolution of at least 10 km must become operational. The U.S. Navy recently increased their global NOGAPS model resolution from approximately 100 km to 50 km. This increase may show some intermediate scale features, but it will still miss or heavily alias

the small near-shore wind curl bands found in this study. A more immediate answer to this problem is a regional model run within the grid structure of a global model.

Regional models like the Navy's COAMPS or the NOAA Eta are now being used in select areas at approximately 15 to 25 km resolutions, and hopefully will soon transition to even higher resolutions. As demand increases, perhaps the Navy will move their 9-km model from research to operational status in some areas. Once that occurs upwelling maps, instead of isolated index sites could be produced for those areas.

The future solution for estimating vertical velocities associated with coastal upwelling may be regional ocean models driven by sub-10-km wind fields. Such regional models provide ideal tools to investigate the ocean's response to patterns of wind stress and wind-stress curl. They can account for important physical variables that are neglected in the present upwelling indices, such as air-sea temperature difference, ocean stability, thermocline depth, and thermocline strength. Also, these ocean models can be linked to nutrient-phytoplankton-zooplankton models and thus provide estimates of the biological effectiveness of upwelling. Ultimately, such estimates might provide researchers with indices of ocean condition that explain more directly and mechanistically the production of fisheries resources. Field experiments are necessary to support and validate these modeling studies. Observations could confirm assumed relationships between physical variables, upwelling, and productivity. Such field operations would require high-resolution ship or fixed-mooring measurements of many variables including the difficult-to-determine vertical velocity of the ocean. This will necessitate a more comprehensive physical and biological observational program for the U.S. west coast.

THIS PAGE INTENTIONALLY LEFT BLANK

LIST OF REFERENCES

Abbott, M. R., and B. Barksdale, Phytoplankton pigment patterns and wind forcing off central California, *J. Geophys. Res., 96*, 14,649-14,667, 1991.

Ainley, D. G., W. J. Sydeman, and J. Norton, Upper trophic level predators indicate interannual negative and positive anomalies in the California Current food web, *Mar. Ecol. Prog. Ser.,* 118, 69-79, 1995.

Allen, J. S., Upwelling and coastal jets in a continuously stratified ocean, *J. Phys. Oceanorgr., 3*, 245-257, 1973.

Atlas, R., S.C. Bloom, R.N. Hoffman, E. Brin, J. Ardizzone, J. Terry, D. Bungato, and J.C. Jusem, Geophysical validation of NSCAT winds using atmospheric data and analyses, *J. Geophys. Res.,* 104, 11,405-11,424, 1999.

Bakun, A., Coastal upwelling indices, west coast of North America, 1946-71, *Tech. Rep. NMFS SSRF-671*, 103 pp., Nat. Oceanic and Atmos. Admin., Seattle, Wash., 1973.

Bakun, A., and R. H. Parrish, Turbulence, transport, and pelagic fish in the California and Peru Current systems, *Calif. Coop. Oceanic Fish. Invest. Rep.,* 23, 99-112, 1982.

Bakun, A., and C. S. Nelson, The seasonal cycle of wind-stress curl in subtropical eastern boundary current regions, *J. Phys. Oceanogr., 21*, 1815-1834, 1991.

Beardsley, R.C., C.E. Dorman, C.A. Friehe, L.K. Rosenfeld, and C.D. Winant, Local atmospheric forcing during the Coastal Ocean Dynamics Experiment 1. A description of the marine boundary layer and atmospheric conditions over a northern California upwelling region, *J. Geophys. Res.,* 92, 1467-1488, 1987.

Blanco, J. L., A. C. Thomas, M. –E. Carr, and P. T. Strub, Seasonal climatology of hydrographic conditions in the upwelling region off northern Chile, *J. Geophys. Res*., 106, 11,451-11,467, 2001.

Borja, A., A. Uriarte, and J. Egana, Environmental factors and recruitment of mackerel, *Scomber scombrus* L. 1758, along the north-east Atlantic coasts of Europe, *Fish. Oceanogr*., 11, 116-127, 2002.

Botsford, L. W., C. A. Lawrence, E. P. Dever, A. Hastings, and J. Largier, Wind strength and biological productivity in upwelling systems: an idealized study, *Fish. Oceanogr.,* 12, 245-259, 2003.

Brink, K. H., D. Halpern, A. Huyer, and R. L. Smith, The physical environment of the Peruvian upwelling system, *Prog. Oceanog*., 12, 285-305, 1983.

Brodeur, R. D. and D. M. Ware, Long-term variability in zooplankton biomass in the subarctic Pacific Ocean, *Fish. Oceanogr.,* 1, 32-38, 1992.

Burk, S. D., and W. T. Thompson, The summertime low-level jet and marine boundary layer structure along the California coast, *Mon. Wea. Rev., 124*, 668-686, 1996.

Burk, S. D., T. Haack, and R. M. Samelson, Mesoscale simulation of supercritical, subcritical, and transcritical flow along coastal topography, *J. Atmos. Sci., 56*, 2780-2795, 1999.

Casey, R. E., T. L. Carson, and A. L. Weinheimer, The modern California current system and radiolarian responses to "normal" (anti-El Nino) conditions, In: Siliceous microfossil and microplankton of the Monterey formation and modern analogs. R. E. Casey and J. A. Barron (eds.), *Pacific Sec. Soc. Econ. Paleontol. And Mineral*., pp. 1-7, 1986.

Chao, Y., Z. Li, J. C. Kindle, J. D. Paduan, and F. P. Chavez, A high-resolution surface vector wind product for coastal oceans: Blending satellite scatterometer measurements with regional mesoscale atmospheric model simulations, *Geophys. Res. Lett., 30(1)*, 1013, doi:10.1029/2002GL015729, 2003.

Chelton, D. B., Large-scale response of the California Current to forcing by the wind stress curl, Calif. Coop. Oceanic Fish. Invest. Rep., 23, 130-148, 1982.

Chereskin, T. K., Direct evidence for an Ekman balance in the California Current, *J. Geophys. Res*., 100, 18,261-18,269, 1995.

Cressman, G., An operational objective analysis system, *Mon. Wea. Rev.,* 87, 367-374, 1959.

Cui, Z., M. Tjernstrom, and B. Grisogono, Idealized simulations of atmospheric coastal flow along the central coast of California, *J. App. Met., 37*, 1332-1363, 1998.

Cury, P., and C. Roy, Optimal environmental window and pelagic fish recruitment success in upwelling areas, *Can. J. Fish. Aquat. Sci.,* 46, 670-680, 1989.

Davidson, K. L., Observational results on the influence of stability and wind-wave coupling on momentum transfer and turbulent fluctuations over ocean waves. *Boundary-Layer Met*. 6, 305-331, 1974.

Dixon, W.J., and F.J. Massey, *Introduction to statistical analysis*, McGraw-Hill, Inc., 638 pp., 1969.

Dorman, C. E., A. G. Enriquez, and C. A. Friehe, Structure of the lower atmosphere over the northern California coast during winter, *Mon. Wea. Rev., 123,* 2384-2404, 1995.

Dorman, C. E., T. Holt, D. P. Rogers, and K. Edwards, Large-scale structure of the June-July 1996 marine boundary layer along California and Oregon, *Mon. Wea. Rev., 128,* 1632-1652, 2000.

Dorman, C. E., D. P. Rogers, W. Nuss, and W. T. Thompson, Adjustment of the summer marine boundary layer around Point Sur, California, *Mon. Wea. Rev., 127,* 2143-2159, 1999.

Dorman, C.E., and C. D. Winant, Buoy observations of the atmosphere along the west coast of the United States, 1981-1990, *J. Geophys. Res.,* 100, 16,029-16,044, 1995.

Ebuchi, N., H. C. Graber, and M. J. Caruso, Evaluation of wind vectors observed by QuikSCAT/SeaWinds using ocean buoy data, *J. Atmos. Oceanic Technol.*, 19**,** 2049-2062, 2002.

Ekman, V. W., On the influence of the earth's rotation on ocean currents. *Ark. Mat. Astron. Fys*., 2, 1-53, 1905.

Enriquez, A. G., and C. A. Friehe, Effects of wind stress and wind stress curl variability on coastal upwelling, *J. Phys. Oceanogr., 25*, 1651-1671, 1995.

Fofonoff, N. P., Machine computations of mass transports in the North Pacific Ocean, *J. Fish. Res. Bd. Canada,* 19, 1121-1141, 1962.

Food and Agriculture Organization of the United Nations, *Yearbook of Fisheries statistics: Catches and landings, Vol. 80*, Viale delle Terme di Caracalla, 00100 Rome, Italy, 713 pp., 1995.

Freilich, M.H., and R.S. Dunbar, The accuracy of the NSCAT vector winds: Comparisons with National Data Buoy Center buoys, *J. Geophys. Res.,* 104, 11,231-11,246, 1999.

Gargett, A. E., The optimal stability 'window': a mechanism underlying decadal fluctuations in North Pacific salmon stocks?, *Fish. Oceanogr.,* 6, 109-117, 1997.

Gilhousen, D.B., A field evaluation of NDBC moored buoy winds, *J. Atmos. Oceanic Technol.*, 4, 94-104, 1987.

Gill, A. E., *Atmosphere-Ocean Dynamics*, Academic, San Diego, Calif., 1982.

Haack, T., S. D. Burk, C. Dorman, and D. Rogers, Supercritical flow interaction within the Cape Blanco-Cape Mendocino orographic complex, *Mon. Wea. Rev., 129*, 688-708, 2001.

Halliwell, G.R. and J. S. Allen, The large-scale coastal wind field along the west coast of North America, 1981-1982, *J. Geophys. Res.,* 92, 1861-1884, 1987.

Halpern, D., Measurements of near-surface wind stress over an upwelling region near the Oregon coast, *J. Phys. Oceanogr., 6*, 108-112, 1976a.

Halpern, D., Structure of a coastal upwelling event observed off Oregon during July 1973, *Deep-Sea Res., 23*, 495-508, 1976b.

Hamilton, G. D., NOAA Data Buoy Office programs, *Bull, Am. Meteorol. Soc., 61*, 1012-1017, 1980.

Hickey, B. M., The California Current System – hypotheses and facts, *Prog. Oceanog., 8*, 191-279, 1979.

Hodur, R. M., The U.S. Navy's Coupled Ocean/Atmosphere Model (COAMPS), *Mon. Wea. Rev., 125*, 1414-1430, 1997.

Hogan, T. F., and L. R. Brody, Sensitivity studies of the Navy's global forecast model parameterizations and evaluation of improvements to NOGAPS, *Mon. Wea. Rev.,* 121, 2373-2395, 1993.

Hogan, T. F., and T. E. Rosmond, The description of the Navy Operational Global Atmospheric Prediction System's spectral forecast model, *Mon. Wea. Rev.,* 119, 1786-1815, 1991.

Hsieh, W. W., D. M. Ware, and R. E. Thomson, Wind-induced upwelling along the west coast of North America, 1899-1988, *Can. J. Fish. Aquat. Sci*., 52, 325-334, 1995.

Huddleston, J. N., and B. W. Stiles, Multidimensional Histogram (MUDH) rain flag product description, version 2.1, Jet Propulsion Lab., Pasadena, Calif., 8pp., 2000. [Available online at http://podaac.jpl.nasa.gov/quikscat/qscat_doc.html.] December 2003.

Huyer, A., Coastal upwelling in the California Current system, Prog. Oceanog., 12, 259-284, 1983.

Huyer, A. and P.M. Kosro, Mesoscale surveys over the shelf and slope in the upwelling region near Point Arena, California, *J. Geophys. Res.,* 92, 1655-1681, 1987.

Huyer, A., R. L. Smith, and T. Paluszkiewicz, Coastal upwelling off Peru during normal and El Nino times, 1981-1984, *J. Geophys. Res.,* 92, 14,297-14,307, 1987.

Jet Propulsion Laboratory, QuikSCAT science data product user's manual, version 2.2, *Publ. D-18053*, 89 pp., 2001, Jet Propulsion Lab., Pasadena, Calif., [Available online at http://podaac.jpl.nasa.gov/quikscat/qscat_doc.html], December 2003.

Kelly, K. A., The influence of winds and topography on the sea surface temperature patterns over the northern California slope*, J. Geophys. Res., 90*, 11,783-11,798, 1985.

Kindle, J. C., R. Hodur, S. deRada, J. Paduan, L. Rosenfeld, and F. Chavez, A COAMPS reanalysis for the Eastern Pacific: Properties of the diurnal sea breeze along the central California coast, *Geophys. Res. Lett., 29(24)*, 2203, doi:10.1029/2002GL015566, 2002.

Koch, S., M. Desjardins, and P. Kocin, An interactive Barnes objective map analysis scheme for use with satellite and conventional data, *J. Clim. Appl. Meteor.,* 22, 1487-1503, 1983.

Koracin, D., and C. E. Dorman, Marine atmospheric boundary layer divergence and clouds along California in June 1996, *Mon. Wea. Rev., 129*, 2040-2056, 2001.

Koslow, J. A., A. J. Hobday, and G. W. Boehlert, Climate variability and marine survival of coho salmon (*Oncorhynchus kisutch*) in the Oregon production area, *Fish. Oceanogr.,* 11, 65-77, 2002.

Kuo, N. J., Q. Zheng, and C. R. Ho, Satellite observations of upwelling along the western coast of the South China Sea, *Remote Sen. Environ*., 74, 463-470, 2000.

Large, W. G., and S. Pond, Open ocean momentum flux measurements in modern to strong winds. *J. Phys. Oceanogr*., 11, 324-336, 1981.

Lentz, S. J., The surface boundary layer in coastal upwelling regions, *J. Phys. Oceanogr*., 22, 1517-1539, 1992.

Liu, W.T., and W. Tang, Equivalent Neutral Wind, Publ. 96-17, Jet Propulsion Lab., Pasadena, Calif., 16pp., 1996. [Available online at http://airsea-www.jpl.nasa.gov/publications.html.] December 2003.

Liu, W.T., W. Tang, and P. S. Polito, NASA scatterometer provides global ocean-surface wind fields with more structures than numerical weather prediction, *Geophys. Res. Lett*., 25, 761-764, 1998.

Liu, W.T., X. Xie, and P.S. Polito, Atmospheric manifestation of tropical instability wave observed by QuikSCAT and Tropical Rain Measuring Mission, *Geophys. Res. Lett*., 27, 2545-2548, 2000.

Long, D. E., and J. M. Mendel, Identifiability in wind estimation from wind scatterometer measurements, *IEEE Trans. Geosci. Remote Sens.,* 29, 268-276, 1991.

McConnaughey, R. A., D. A. Armstrong, B. M. Hickey, and D. R. Gunderson, Juvenile Dungeness crab (*Cancer magister*) recruitment variability and oceanic transport during the pelagic larval phase, *Can. J. Fish. Aquat. Sci*., 49, 2028-2044, 1992.

Mears, C.A., D.K. Smith, and F.J. Wentz, Detecting rain with QuikSCAT, *International Geoscience and Remote Sensing Symposium Proceedings*, Honolulu, Hawaii, July 2000, IEEE, 1235-1237, 2000.

Mears, C.A., D.K. Smith, and F.J. Wentz, Comparison of Special Sensor Microwave Imager and buoy-measured wind speeds from 1987 to 1997, *J. Geophys. Res.,* 106**,** 11,719-11,729, 2001.

Mueter F. J., D. M. Ware, and R. M. Peterman, Spatial correlation patterns in coastal environmental variables and survival rates of salmon in the north-east Pacific Ocean, *Fish. Oceanogr.,* 11, 205-218, 2002.

Muller, E. M., and D. M. Figueroa, Spatial and seasonal distribution of wind stress over the sea off continental Chile using ship data, *Cienc. Tec. Mar*., 19, 7-17, 1996.

Murphy, A. H., and E. S. Epstein, Skill scores and correlation coefficients in model verification, *Mon. Wea. Rev*., 117, 572-581, 1989.

NASA, SeaWinds on QuikSCAT, cited 2002. [Available online at http://podaac.jpl.nasa.gov/quikscat.]

Nelson, C. S., Wind stress and wind-stress curl over the California Current, *Tech. Rep. NMFS SSRF-714*, 87pp., Nat. Oceanic and Atmos. Admin., Seattle, Wash., 1977.

NOAA, Ocean surface winds derived from the SeaWinds scatterometer. [Available online at http://manati.wwb.noaa.gov/quikscat.] December 2003.

Norton, J. G., F. B. Schwing, M. H. Pickett, S. G. Cummings, D. Husby, and P. Green Jessen, Monthly mean coastal upwelling indices, west coast of South Africa 1981 to 2000: Trends and relationships, *Tech. Rep. NOAA-TM-NMFS-SWFSC-343,* 37pp., Nat. Oceanic and Atmos. Admin., Seattle, Wash., 2002.

Norton, J. G., F. B. Schwing, M. H. Pickett, D. Husby, and C. S. Moore, Monthly mean coastal upwelling indices, west coast of South America 1981 to 2000: Trends and relationships, *Tech. Rep. NOAA-TM-NMFS-SWFSC-316*, 35pp., Nat. Oceanic and Atmos. Admin., Seattle, Wash., 2001.

Parrish, R. H., and D. L. Mallicoate, Variation in the condition factors of California pelagic fishes and associated environmental factors, *Fish. Oceanogr*., 4, 171-190, 1995.

Patoux, J., and R.A. Brown, A scheme for improving scatterometer surface wind fields, *J. Geophys. Res.,* 106, 23,985-23,994, 2001.

Pickett, M. H., and J. D. Paduan, Ekman transport and pumping in the California Current based on the U.S. Navy's high-resolution atmospheric model (COAMPS), *J. Geophys. Res.,* 108(C10), 3327, doi:10.1029/2003JC001902, 2003.

Pickett, M. H., W. Tang, L. K. Rosenfeld, and C. H. Wash, QuikSCAT satellite comparisons with near-shore buoy wind data off the US west coast, *J. Atmos. Oceanic Technol.,* 20, 1869-1879, 2003.

Portabella, M., and A. Stoffelen, Rain detection and quality control of SeaWinds, *J. Atmos. Oceanic Technol.*, 18, 1171-1183, 2001.

Rosenfeld, L. K., F. B. Schwing, N. Garfield, and D. E. Tracy, Bifurcated flow from an upwelling center: a cold water source for Monterey Bay, *Cont. Shelf Res., 14*, 931-964, 1994.

Rudnick, D. L., and R. E. Davis, Mass and heat budgets on the northern California continental shelf, *J. Geophys. Res., 93*, 14,013-14,024, 1988.

Ryding, K. E. and J. R. Skaliski, Multivariate regression relationships between ocean conditions and early marine survival of coho salmon (*Oncorhynchus kisutch*), *Can. J. Fish. Aquat. Sci*., 56, 2374-2384, 1999.

Samelson, R., P. Barbour, J. Barth, S. Bielli, T. Boyd, D. Chelton, P. Kosro, M. Levine, E. Skyllingstad, and J. Wilczak, Wind stress forcing of the Oregon coastal ocean during

the 1999 upwelling season, *J. Geophys. Res., 107*(C5), 3034, doi:10.1029/2001JC000900, 2002.

Schlax, M.G., D.B. Chelton, and M.H. Freilich, Sampling errors in wind fields constructed from single and tandem scatterometer data sets, *J. Atmos. Oceanic Technol.*, 18, 1014-1036, 2001.

Schwing, F. B., M. O'Farrell, J. Steger, and K. Baltz, Coastal upwelling indices, west coast of North America 1946-1995, *Tech. Rep. NOAA-TM-NMFS-SWFSC-231*, 207pp., Nat. Oceanic and Atmos. Admin., Seattle, Wash., 1996.

Shaffer, S. J., R. S. Dunbar, S. V. Hisao, and D. G. Long, A median-filter-based ambiguity removal algorithm for NSCAT, *IEEE Trans. Geosci. Remote Sens*., 29, 167-174, 1991.

Shaffer, G., S. Hormazabal, O. Pizarro, and S. Salinas, Seasonal and interannual variability of currents and temperature off central Chile, *J. Geophys. Res.,* 104, 29,951-29,961, 1999.

Smith, R. L., Upwelling, *Oceanogr. Mar. Biol. Ann. Rev., 6*, 11-46, 1968.

Smith, R. L., A comparison of the structure and variability of the flow field in three coastal upwelling regions: Oregon, North-west Africa, and Peru, *Coastal Upwelling*, F. A. Richards, Ed., Amer. Geophys. Union, 107-118, 1981.

Smith, R. L., A. Huyer, J. S. Godfrey, and J. A. Church, The Leeuwin current off Western Australia, 1986-1987, *J. Phys. Oceanogr*., 21, 323-345, 1991.

Smith, S.D., Coefficients for sea surface wind stress, heat flux, and wind profiles as a function of wind speed and temperature, *J. Geophys. Res.*, 93, 15,467-15,472, 1988.

Spencer, M.W., C. Wu, and D.G. Long, Improved resolution back scatter measurements with the SeaWinds pencil-beam scatterometer, *IEEE Trans. Geosci. Remote Sens.*, 38, 89-103, 2000.

Stenevik, E. K., M. Skogen, S. Sundby, and D. Boyer, The effect of vertical and horizontal distribution on retention of sardine (*Sardinops sagax*) larvae in the Northern Benguela – observations and modeling, *Fish. Oceanogr.*, 12, 185-200, 2003.

Stiles, B. W., B. D. Pollard, and R. S. Dunbar, Direction interval retrieval with thresholded nudging: A method for improving the accuracy of QuikSCAT winds, *IEEE Trans. Geosci. Remote Sens.*, 40, 79-89, 2002.

Strub, P. T., C. James, A. C. Thomas, and M. R. Abbott, Seasonal and nonseasonal variability of satellite-derived surface pigment concentration in the California Current, *J. Geophys. Res., 95*, 11,501-11,530, 1990.

Sverdrup, H. U., M. W. Johnson, and R. H. Fleming, *The Oceans: Their Physics, Chemistry, and General Biology,* 1087 pp., Prentice-Hall, Englewood Cliffs, NJ, 1942.

Tang, W., and W.T. Liu, Objective interpolation of scatterometer winds, Publ. 96-19, Jet Propul. Lab., Pasadena, Calif., 16 pp., 1996. [Available online at http://airsea-www.jpl.nasa.gov/publications.html.] December 2003.

Thomson, R. E., and D. M. Ware, A current velocity index of ocean variability, *J. Geophys. Res., 101*, 14,297-14,310, 1996.

Tjernstrom, M., and B. Grisogono, Simulations of supercritical flow around points and capes in a coastal atmosphere, *J. Atmos. Sci., 57*, 108-135, 2000.

Trenberth, K. E., W. G. Large, and J. G. Olson, The mean annual cycle in global ocean wind stress, *J. Phys. Oceanogr*., 20, 1742-1760, 1990.

Von Storch, H., and F. W. Zwiers, *Statistical Analysis in Climate Research*, Cambridge University Press, Madrid, Spain, pp. 391-406, 1999.

Ward, M. N., and B. J. Hoshkins, Near-surface wind over the global ocean 1949 – 1988, *J. Climate,* 9, 1877-1895, 1996.

Wickett, W. P., Ekman transport and zooplankton concentration in the North Pacific Ocean, *J. Fish. Res. Bd. Canada,* 24, 581-594, 1967.

Winant, C.D., R.C. Beardsley, and R.E. Davis, Moored wind, temperature, and current observations made during Coastal Ocean Dynamics experiments 1 and 2 over the northern California continental shelf and upper slope, *J. Geophys. Res.*, 92, 1569-1604, 1987.

Winant, C. D., and C. E. Dorman, Seasonal patterns of surface wind stress and heat flux over the Southern California Bight, *J. Geophys. Res., 102*, 5641-5653, 1997.

Winant, C. D., C. E. Dorman, C. A. Friehe, and R. C. Beardsley, The marine layer off northern California: An example of supercritical channel flow, *J. Atmos. Sci.,* 45, 3588-3605, 1988.

Wooster, W. S., and J. L. Reid, Eastern boundary currents, *The Sea*, Vol. 2, Interscience Pub., New York, pp. 253-280, 1963.

Xie, L., and W. M. Hsieh, The global distribution of wind-induced upwelling, *Fish. Oceanogr*., 4, 52-67, 1995.

Xie, S.P., W.T. Liu, Q. Liu, and M. Nonaka, Far-reaching effects of the Hawaiian Islands on the pacific ocean-atmosphere system, *Science*, 292, 2057-2060, 2001.

Yoshida, K., Coastal upwelling off the California coast, *Rec. Oceanogr. Works Japan, 2,* 8-20, 1955.

INITIAL DISTRIBUTION LIST

1. Defense Technical Information Center
   Ft. Belvoir, Virginia

2. Dudley Knox Library
   Naval Postgraduate School
   Monterey, California

3. Maury Library
   Naval Oceanographic Office
   Stennis Space Center, Mississippi

4. PFEL Library
   NOAA/Pacific Fisheries Environmental Laboratory
   Pacific Grove, California

5. Dr. Curtis A. Collins
   Department of Oceanography
   Naval Postgraduate School
   Monterey, California

6. Dr. Franklin B. Schwing
   NOAA/Pacific Fisheries Environmental Laboratory
   Pacific Grove, California

7. Dr. Leslie K. Rosenfeld
   Department of Oceanography
   Naval Postgraduate School
   Monterey, California

8. Dr. Jeffrey D. Paduan
   Department of Oceanography
   Naval Postgraduate School
   Monterey, California

9. Dr. Carlyle H. Wash
   Department of Meteorology
   Naval Postgraduate School
   Monterey, California

10. Dr. Michael R. Laurs
    NOAA/Pacific Fisheries Environmental Laboratory
    Pacific Grove, California

11. Dave Foley
NOAA/Pacific Fisheries Environmental Laboratory
Pacific Grove, California

12. Dr. Clive Dorman
Department of Geological Sciences
San Diego State University
San Diego, California